# Noisy Blurred Image Restoration Based on Noise Variance Estimation in Blind Condition

Chong Yi

A Dissertation Submitted to
the Graduate School of Science and Engineering
in Partial Fulfillment of the Requirements for the Degree of
DOCTOR OF ENGINEERING
in
Mathematics, Electronics and Informatics

Supervisor: Professor Tetsuya Shimamura

Saitama University, Japan

March 2014

# Contents

# List of Figures

# List of Tables

# Nomenclature

| | |
|---|---|
| $g$ | degraded image |
| $f$ | original image |
| $h$ | point-spread function |
| $a$ | AR model coefficients |
| $e$ | AR model error |
| $n$ | Gaussian noise |
| $\sigma_e^2$ | variance of AR model error |
| $\sigma_n^2$ | variance of Gaussian noise |
| $L(\theta)$ | log-likelihood function |
| $p(g;\theta)$ | probability density function of $g$ |
| $\boldsymbol{P}$ | covariance matrix of $g$ |
| $\boldsymbol{V}$ | covariance of $f$ |
| $\boldsymbol{R}_{ff}$ | conditional autocorrelation matrix |
| $\boldsymbol{R}_{fg}$ | cross-correlation matrix |
| $L$ | length of motion |
| $\phi$ | angle of motion direction |
| $R$ | radius of uniform blur |
| $\sigma_G^2$ | Gaussian blur variance |

| | |
|---|---|
| $H_m$ | homogeneity measure |
| $PSNR_{B_r}$ | reference PSNR |
| $PSNR_{B_{ij}}$ | PSNR of a certain block |
| $t_{PSNR}$ | threshold for homogeneous block selection |
| $\sigma^2_{B_r}$ | reference variance |
| $\sigma^2_{B_{ij}}$ | variance of a certain block |
| $t_D$ | threshold for homogeneous block selection |
| $\mu_{R_{PSNR}}$ | average of the estimation results |
| $R_{PSNR}$ | noise variance estimation result |
| $T_{PSNR}$ | true value of PSNR |
| $N$ | the number of images |
| $M$ | the number of estimations |
| $H$ | Hessian matrix |
| $f_{xx}$ | second-order derivatives of xx directions |
| $f_{xy}$ | second-order derivatives of xy directions |
| $f_{yy}$ | second-order derivatives of yy directions |
| $\lambda_1$ | maximum local variation |
| $\lambda_2$ | minimum local variation |
| $I(f)$ | difference eigenvalue edge indicator |
| $w(f(x,y))$ | weighting parameter |
| $\theta$ | constant |

| | |
|---|---|
| $\sigma^2(x, y)$ | gray-level variance |
| $\sigma^2_{B_s}$ | variance of the selected homogeneous blocks |
| $\mu_{\sigma^2_{B_s}}$ | averaged variance of the selected homogeneous blocks |

# Acknowledgements

This thesis is the results of three years work whereby I have been accompanied and supported by many people. It is a pleasant aspect that I have now the opportunity to express my gratitude for all of them.

First and foremost, I would like to record my gratitude to Professor Tetsuya Shimamura for his great supervision, advice and guidance from the very early stage of this research. His overly enthusiasm as a principle-centered person and integral view on research has made a deep impression on me.

Next, I would like to thank to my committee members for their precious time and valuable suggestions in my thesis proposal defense.

Last, I would like to grateful acknowledge for the encouragement, supports and sacrifices of my parents and wife during I study at Saitama University and sincerely dedicate this work to them.

# Abstract

Many image restoration algorithms have been proposed over the last few decades. But in early work on image restoration, it was nearly always assumed that all the information required to restore an image is known previously. Unfortunately, this is not possible in most real-life situations. Thus, the technique of blind image restoration estimating both the true image and the blur from a degraded image has been researched. However, when taking noise into account, the estimation problem becomes more challenging. Estimating the blue and noise parameters simultaneously may cause a large estimation error.

To minimize the estimation error, we propose a Maximum-Likelihood Estimation Algorithm based on noise variance estimation. This method estimates the noise variance only using the information from the known degraded image. This improves the estimation accuracy significantly.

For better results for noise variance estimation from the degraded image, we propose a structure-based method. This method separates an image into blocks. Rejecting the edge included blocks, only the homogenous blocks are selected for the noise estimation process. Since image details can be better revealed by second-order operators, for better estimation, we further propose a difference eigenvalue edge indicator with threshold for more accurate block selection.

After combining the noise estimation method, better estimation results of blur and noise are derived, leading to the better restoration results. Experiments show that the structure-based method is good for light noisy condition, while the difference eigenvalue based method is effective for fine texture images.

Chapter 1

# 1 Introduction

The goal of image restoration is to reconstruct the original scene from a degraded observation [1]. This recovery process is critical to many image processing applications. Although classical linear image restoration has been thoroughly studied [2], [3], the more difficult problem of blind image restoration has numerous research possibilities.

Blind image restoration is the process of estimating both the true image and the blur from the degraded image characteristics, using partial information about the imaging system. In classical linear image restoration, the blurring function is given, and the degradation process is inverted using one of the many known restoration algorithms. The various approaches that have appeared in the literature depend upon the particular degradation and image models [2], [3].

Deconvolution is performed for image restoration in many applications such as astronomical speckle imaging [4], remote sensing [5], and medical imaging [6]-[9], among others. In most situations, the point-spread function (PSF) is assumed to be known explicitly prior to the deconvolution procedure. This problem is known as the classical linear image restoration problem. The long list of deconvolution methods for this situation includes a variety of well known techniques, such as inverse filtering, Wiener filtering, least-squares filtering, recursive Kalman filtering, and constrained iterative deconvolution methods [2], [10]-[13].

Unfortunately, in many practical situations, the blur is often unknown, and little information is available about the true image. Therefore, the true image must be identified directly from the degraded image by using partial or no information about the blurring process and the true image. Such an estimation problem, assuming the linear degradation model is called blind deconvolution. Experience shows that in practice

some information is needed to successfully restore the image.

There are several motivating factors behind the use of blind deconvolution for image processing applications. In practice, it is often costly, dangerous, or physically impossible to obtain a priori information about the imaged scene. For example, in applications like remote sensing and astronomy, it is difficult to statistically model the original image or even know specific information about scenes never imaged before [4], [5]. In addition, the degradation from blurring cannot be accurately specified. In aerial imaging and astronomy, the blurring cannot be accurately modeled as a random process, since fluctuations in the PSF are difficult to characterize [14]. In real-time image processing, such as medical video-conferencing, the parameters of the PSF cannot be pre-determined to instantaneously deblur images [15]. Moreover, on-line identification techniques used to estimate the degradation may result in significant error, which can create artifacts in the restored image [16].

In other applications, the physical requirements for improved image quality are unrealizable. For instance, in space exploration, the physical weight of a high resolution camera exceeds practical constraints. Similarly, in x-ray imaging, improved image quality occurs with increased incident x-ray beam intensity, which is hazardous to a patient's health [6]. Thus, blurring is unavoidable. In such situations, the hardware available to measure the PSF of an imaging system is often difficult to use. Although these methods work well to identify the PSF, they are esoteric, which limits their wide use [9], [14]. Blind deconvolution is a viable alternative for improving image quality without requiring complicated calibration methods.

Finally, for applications such as astronomy, adaptive-optics systems may be used to compensate for blurring degradations, although the high cost of these systems makes imaging impractical for some observational facilities. Use of less expensive, partially compensating systems may result in phase errors. In either situation, post-processing such as blind deconvolution is required for improved image quality [17], [18].

It is clear that classical image restoration methods that assume a known PSF are not suitable for many real image processing situations. In these cases, an algorithmic approach to combine blur identification and image restoration is required. In this sense, blind deconvolution is a practical method for image restoration. Indeed, existing research in the area [9], [14], [16], has shown its worth.

## 1.1 Problem Formulation

In many imaging applications, an observed image *g(x,y)*, neglecting additive noise, can be assumed to be the two-dimensional convolution of the true image *f(x,y)* with a linear shift-invariant blur, also known as the PSF, *h(x,y)*. That is,

$$\begin{aligned} g(x,y) &= f(x,y) * h(x,y) \\ &= \sum_{(n,m)} f(n,m)h(x-n, y-m), \\ x, y, n, m &\in Z \end{aligned} \tag{1.1}$$

In which * denotes the two-dimensional linear convolution operator, and Z is the set of integer numbers. The problem of recovering the true image *f(x,y)* requires the deconvolution of the PSF *h(x,y)*, from the degraded image *g(x,y)*.

The general blind deconvolution problem refers to the task of separating two convolved signals, *f* and *h*, when both the signals are either unknown or partially known. This important problem occurs in many applications in addition to image restoration, such as seismic data analysis, blind equalization of communication channels, transmission monitoring, and echo cancellation in wireless telephony [19]-[22]. The basic approach for all cases involves using the partial information available about the scheme as a reference to deconvolve the received signal components. The partial information can be in the form of physical properties of the true signal, such as finite support and nonnegativity found in image processing, or it can be in the form of statistical information such as entropy used for seismic data analysis, or the probability density function (PDF) of the true signal used for equalization of communication channels. In most blind deconvolution techniques, the partial information is incorporated into an optimality criterion, which is minimized (or maximized) to find estimates of the components (or their inverses). Figure 1.1 depicts the general blind deconvolution scenario.

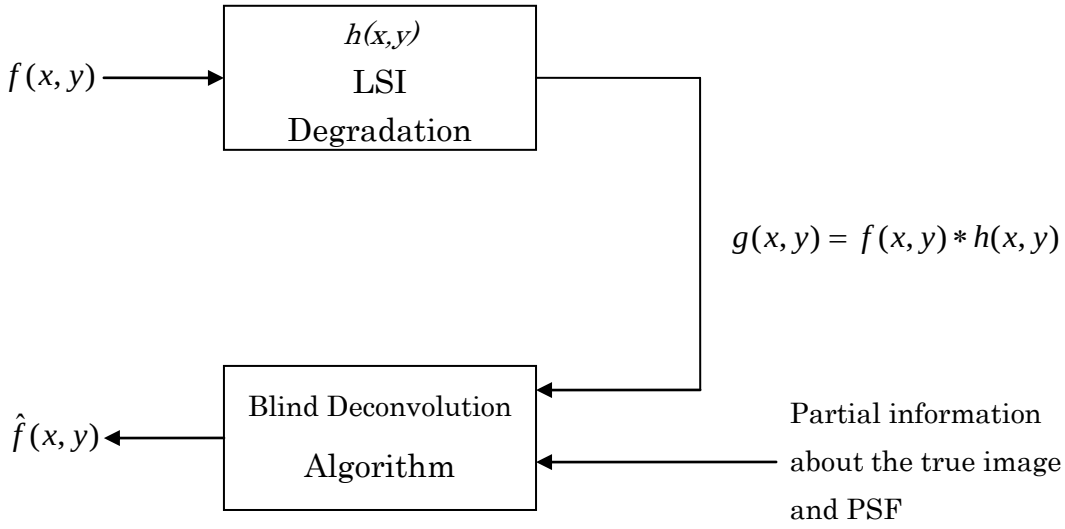


Figure 1.1: Blind deconvolution process

## 1.2 Important Characteristics of Blind Deconvolution

There are some important characteristics and practical constraints for the problem of blind deconvolution process. These include:

1. The true image and PSF must be irreducible for an unambiguous deconvolution. An irreducible signal is one which cannot be exactly expressed as the convolution of two or more component signals, on the understanding that the two-dimensional delta function is not a component signal. This is an important property of the system because if either the true image or the PSF are reducible then the solution to the problem is ambiguous.
2. The image restoration problem is, in general, ill-conditioned; a small perturbation of the given data produces large deviations in the resulting solution.
3. Exact deconvolution is impossible as a result of the presence of additive noise in the imaging system.
4. The solution may not be unique. Since only partial information about the imaging process is used to formulate an optimality criterion, many different estimates of the true image and PSF may lead to an optimal solution.

5. There exists a poor compromise among computational complexity, convergence properties, and portability of the algorithm for the existing blind deconvolution methods.

## 1.3 Existing Approaches in Blind Deconvolution

There are two main approaches to blind deconvolution of images:

1. Identifying the PSF separately from the true image, in order to use it later with one of the known classical image restoration methods. Estimating the PSF and the true image are disjoint procedures. This approach leads to computationally simple algorithms.
2. Incorporating the identification procedure with the restoration algorithm. This merge involves simultaneously estimating the PSF and the true image, which leads to the development of more complex algorithms.

This Section discusses every class of algorithms. Among them, a priori blur identification methods fall under the first approach, and the remaining methods are the second.

### 1.3.1 Zero Sheet Separation

The method of zero sheets has received attention because it provides valuable insight into the blind deconvolution problem in multiple dimensions. Lane and Bates [23] have shown that any degraded image, formed by convolving several individual components, having compact support, is automatically deconvolvable provided its dimension is greater than one. Their argument rests on the analytic properties of the Z-Transform (ZT) in multiple dimensions. The zeros of the ZT of a K-dimensional component is almost always continuous and lies on a (2K-2)-dimensional hyper-surface. The zero sheets can very rarely possess singularities; the relevant details are provided in [24]. By separating these hyper-surfaces, we can recognize the individual components up to a complex scale factor.

### 1.3.2 A Priori Blur Identification Methods

A priori blur identification methods perform blind deconvolution by identifying the PSF prior to restoration. This general class of techniques makes assumptions on the characteristics of the PSFs resulting from linear camera motion or an out-of-focus lens system. Based on these assumptions, an attempt is made to completely characterize the

PSF using special features of the true and blur image [25]-[28].

A priori blur identification techniques are the simplest class of blind deconvolution methods to implement and have low computational requirements. They are applicable to situations in which the true image is known to possess special features, or when the PSF is known to be of a special parametric form. For more general situations or when less information is available, other deconvolution algorithms must be used.

### 1.3.3 ARMA Parameter Estimation Methods

Blind deconvolution using ARMA parameter estimation methods involves modeling the true image as a two-dimensional autoregressive (AR) process and the PSF as a two-dimensional moving average (MA) process. Based on these models, the resulting blurred image is represented as an autoregressive moving average (ARMA) process. Identifying the ARMA parameters allows us to identify the true image and PSF.

The existing methods of this class differ in how the ARMA parameters are estimated. Techniques based on second-order statistics, such as maximum-likelihood (ML) estimation [29]-[32], generalized cross-validation (GCV) [33], and neural networks [34] have been proposed. High order statistics (HOS) methods have also been used for ARMA estimation [35]. The ML and GCV methods are the most successful for image processing applications.

### 1.3.4 Nonparametric Deterministic Image Constraints Restoration Techniques

In contrast to the methods discussed in the previous Sections, the algorithms of this class do not assume parametric models for either the image or the blur. Deterministic constraints such as nonnegativity, known finite supports and existence of blur invariant edges are assumed for the true image. A number of blind deconvolution techniques for images fall into this class, such as the nonnegativity and support constraints recursive inverse filtering (NAS-RIF) algorithm [36], [37], among others.

The methods are iterative and simultaneously estimate the pixels of the true image and PSF. The constraints on the true image and PSF are incorporated into an optimality criterion which is minimized using numerical techniques.

### 1.3.5 Nonparametric Methods Based on High Order Statistics

This class of techniques is structurally similar to the NAS-RIF algorithm, and is useful for restoring texture images [38], [39]. They are based on minimizing the given cost function that accounts for the probabilistic non-Gaussian nature of the true image. The degraded image is passed through an FIR inverse filter, yielding an estimate of the true image. The FIR filter parameters are updated in order to optimize a function that

incorporates the HOS model of the true image.

A well-known technique in this class is minimum entropy deconvolution (MED) [19], which attempts to find the FIR inverse filter of the PSF that yields the smallest output entropy then applied to the degraded image. This technique maximizes the simple “spike-like” character of the true image estimate. This is useful for applications like astronomy, in which the true image is composed of bright spots against a dark background; and geophysics, where teleseismic signals have a spike-like nature. MED has also been proposed for restoring two-tone images [38].

## 1.4 Related Works

Image noise is generally of the following types: Gaussian noise, salt-and-pepper noise, shot noise, quantization noise (uniform noise), film grain and non-isotropic noise. The noise signal can be modeled as a random signal which is additive or multiplicative, signal-dependent or signal-independent, white or colored to an image signal. And most noise variance estimation methods assume that the noise signal is additive Gaussian white noise. Thus, in this paper, we also use this noise model.

The techniques of noise variance estimation are also utilized in the thesis. The related methods and comparisons are introduced in detail in Chapters 3 and 4.

## 1.5 Thesis Organization

The rest of the thesis is organized as follows. Improved maximum-likelihood estimation algorithm for image restoration is presented in Chapter 2. In Chapter 3, improved structure-based Gaussian variance estimation method is presented. This method improves the noise estimation process of the image restoration in Chapter 2. Further more, Chapter 4 derives image noise estimation based on difference eigenvalue, which provides the better choice for the homogenous blocks selection compared with that in Chapter 3. More accurate image restoration results can be expected if utilizing the method in Chapter 4 for the noise estimation process. Finally, Chapter 5 gives conclusion and future works.

Chapter 2

# 2 Improved Maximum-Likelihood Estimation Algorithm for Blind Image Deconvolution Based on Noise Variance Estimation

Restoring an observed image suffering from blur and noise simultaneously is a challenging problem that may cause a large estimation error of blur and noise parameters. In this Chapter, a novel blind image deconvolution approach based on noise variance estimation is presented. This method first performs noise variance estimation from a noisy blurred image. Then, using the property that a certain type of blur may lead to a specific frequency component distortion of the image Fourier spectrum, the blur type can be reorganized. After this, according to the reorganized blur type, the image and blur model coefficients can be computed more efficiently by minimizing an objective function based on the ARMA model. The ML method is the most successful for estimating the ARMA parameters among the existing methods of this class. Because the Exception-Maximization (EM) technique is popular for solving the nonlinear optimization problem in the ML objective function. It converts the original nonlinear optimization problem of several variables into a linear iterative procedure. The restored image is obtained with a least-squares filter. Experiments on images are presented which show that the proposed method is capable of yielding good restoration results.

## 2.1 Related Works

Image restoration is one of the most important research issues in digital image processing. It has been widely applied for medical imaging, astronomical imaging, remote sensing, microscopy imaging, photography deblurring, and so forth [40]. In early work on image restoration, it was nearly always assumed that all the information required to restore an image is known *a priori*. Unfortunately, this is not possible in most real-life situations. Thus, the technique of blind image restoration has been researched.

Blind image restoration is the process of estimating both the true image and the blur from degraded image characteristics using partial information about the imaging system [1]. Most blur is one of three types [41]:

(a) Motion blur, which is the apparent streak of rapidly moving objects in a still image. Liu et al. [42] presented a new approach to motion blur identification based on the Bayesian paradigm and the maximum a posteriori method. Sun et al. [43] estimated the parameters of motion blur (orientation and extension) from the observed image gradients.

(b) Defocus blur, which is generated because of lens defocus. Cui et al. [44] proposed a novel approach to defocus blur image restoration, which is based on global phase coherence. Lee et al. [45] showed how a cellular neural network can be used to estimate defocus blur parameters.

(c) Gaussian blur. Chen and Ma [46] proposed an empirical identification method of the Gaussian blur parameter for image deblurring, in which the estimated parameters are chosen from a collection of candidate parameters. Orieux et al. [47] found the solution of Gaussian blur parameter estimation by inferring a global a posteriori law for the unknown object and parameters.

At present, there are three main classes of methods for blind image restoration: the ARMA parametric approach, the iterative blind deconvolution approach [48], [49], and the multichannel blind restoration approach [50]. In the ARMA model, the AR coefficients determine the image model coefficients, and the MA part determines the PSF of the blurring system. Next, the identification problem can be formulated as an ML problem. Lagendijk et al. [32] presented an ML approach to the blur identification problem and proposed the employment of the EM algorithm to optimize the nonlinear

likelihood function in an efficient way. Tekalp et al. [29] presented a technique of estimating the optimal statistical parameters for the identification of an unknown image and blur model parameters. Deng and Xia [51] developed a neural network algorithm for fast blind image restoration.

When taking noise into account, however, the estimation problem becomes more challenging. Estimating the blur and noise parameters simultaneously may cause a large estimation error. Moreover, some blur identification methods even require that the amount of noise in the observed blurred image is negligible, which is uncommon for practical images of interest. Since there are already efficient algorithms for estimating the noise variance from a noisy image [52]-[54], it is reasonable to pre estimate the noise variance from a noisy blurred image as a pretreatment for the blur identification method. In this Chapter, a novel blind image deconvolution approach based on noise variance estimation and blur type reorganization is presented.

This Chapter is organized as follows. An overview of the parametric blur identification problem is provided in Section 2.2. Noise variance estimation and blur parameter calculation are presented in Section 2.3. Experiments and a summary are given in Section 2.4 and Section 2.5, respectively.

## 2.2 Image Model and Estimation

### 2.2.1 ARMA model

Generally, blind image deconvolution using ARMA parameter estimation methods involves modeling the true image as a two-dimensional (2-D) AR process and the PSF as a 2-D MA process [1]. Based on these models, the resulting blurred image is represented as an ARMA process. Identifying the ARMA parameters allows us to identify the true image and PSF.

The true image is modeled as a 2-D AR process represented by

$$\begin{aligned} f(x,y) &= a(x,y) * f(x,y) + e(x,y) \\ &= \sum_{(k,l)\in R_a} a(k,l) f(x-k, y-l) + e(x,y) \end{aligned} \tag{2.1}$$

where $f(x,y)$ is the true image and $e(x,y)$ is the modeling error, which is assumed

to be a zero-mean homogeneous noise process with covariance matrix $\boldsymbol{Q}_e$, which is statistically independent of $f(x,y)$. $\{a(k,l)\}$ are the AR model coefficients of support $R_a$, which are chosen to minimize the variance of $e(x,y)$, denoted by $\sigma_e^2$.

In most practical situations, the PSF is of finite extent and its effect on the true image can be modeled as that of a 2-D FIR filter. The MA model of a degraded image $g(x,y)$ can be expressed as

$$\begin{aligned} g(x,y) &= h(x,y) * f(x,y) + n(x,y) \\ &= \sum_{(m,n)\in R_h} h(m,n) f(x-m, y-n) + n(x,y) \end{aligned} \tag{2.2}$$

where $R_h$ is the finite support of the PSF $h(m,n)$ and $n(x,y)$ is the additive noise of the imaging system, assumed to be a zero-mean Gaussian with covariance $\boldsymbol{Q}_n$.

A more compact version of (2.4) and (2.5) can be derived by lexicographically ordering the two-dimensional signals and using matrix-vector notation [55]:

$$\boldsymbol{f} = \boldsymbol{A}\boldsymbol{f} + \boldsymbol{e} \tag{2.4}$$

$$\boldsymbol{g} = \boldsymbol{H}\boldsymbol{f} + \boldsymbol{n} \tag{2.5}$$

Rearranging (2.4), substituting into (2.5), and rearranging yields

$$\boldsymbol{g} = \boldsymbol{H}(\boldsymbol{I} - \boldsymbol{A})^{-1}\boldsymbol{e} + \boldsymbol{n} \tag{2.6}$$

where $\boldsymbol{I}$ is the identity matrix. Therefore, we can define the unknown parameter set $\boldsymbol{\theta}$ as a concatenation of four components: $\{a(k,l), \sigma_e^2, h(m,n), \sigma_n^2\}$.

### 2.2.2 ML Estimation Algorithm

In this Section, we choose the ML approach for ARMA parameter estimation, which is the most successful for image processing applications and also has a long history of use with ARMA modeling.

The ML method attempts to derive an estimate of the parameters such that the probability of receiving the observed image, given the parameter set $\theta$, is maximized. The ML estimator [32] is given by

$$\hat{\theta}_{ml} = \arg\min_{\theta\in\Theta}\{\log(\det|\boldsymbol{P}|) + \boldsymbol{g}^T\boldsymbol{P}^{-1}\boldsymbol{g}\} \tag{2.7}$$

where $L(\theta)$ denotes the log-likelihood function of $\theta$, $\Theta$ specifies the range of elements of $\theta$, and $p(g;\theta)$ is the PDF of $\boldsymbol{g}$ for a given $\theta$.

Since $\boldsymbol{e}$ and $\boldsymbol{n}$ are independent Gaussian processes, $\boldsymbol{g}$ is also zero-mean and Gaussian because it is a linearly filtered version of both $\boldsymbol{e}$ and $\boldsymbol{n}$ (see (2.6)). Also, $p(g;\theta)$ is given by

$$p(g;\theta) = \frac{1}{\sqrt{(2\pi)^{N^2}\det|\boldsymbol{P}|}}\exp(-\frac{1}{2}\boldsymbol{g}^T\boldsymbol{P}^{-1}\boldsymbol{g}) \tag{2.8}$$

where $\boldsymbol{P}$ is the covariance matrix of $\boldsymbol{g}$, given by

$$\boldsymbol{P} = \boldsymbol{H}(\boldsymbol{I}-\boldsymbol{A})^{-1}\boldsymbol{Q}_e(\boldsymbol{I}-\boldsymbol{A})^{-T}\boldsymbol{H}^T + \boldsymbol{Q}_n \tag{2.9}$$

By substituting (2.8) into (2.7), the ML blur identification problem can be expressed as follows:

$$\hat{\theta}_{ml} = \arg\min_{\theta\in\Theta}\{\log(\det|\boldsymbol{P}|) + \boldsymbol{g}^T\boldsymbol{P}^{-1}\boldsymbol{g}\} \tag{2.10}$$

Thus, the ML method becomes a method of minimizing this nonlinear objective function with respect to the parameter set $\boldsymbol{\theta}$.

Several implementations exist to solve this nonlinear optimization problem. In this Section, the EM algorithm is used because it converts the nonlinear optimization problem into a linear iterative procedure and is straightforward to implement.

### 2.2.3 EM Algorithm

The EM iterative procedure involves solving linear equations only. The structure is shown in Figure 2.1.

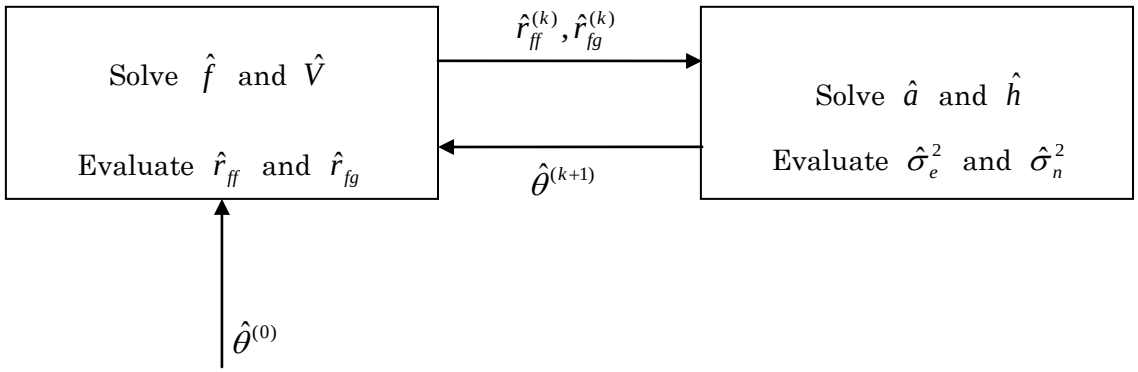


Figure 2.1: Structure of EM blur identification algorithm

As can be seen from Figure 2.1, for the first step, the initial values of the parameter set $\hat{\theta}^{(0)}$ is used to calculate $\hat{\boldsymbol{f}}$ and $\hat{\boldsymbol{V}}$, which denote the conditional mean and covariance of $\boldsymbol{f}$, respectively. $\hat{\boldsymbol{f}}$ and $\hat{\boldsymbol{V}}$ can be expressed as

$$\hat{\boldsymbol{f}} = E(f / g; \hat{\theta}^{(k)}) = \hat{\boldsymbol{V}}\boldsymbol{H}^t\boldsymbol{Q}_n^{-1}\boldsymbol{g} \tag{2.11}$$

$$\hat{\boldsymbol{V}} = \mathrm{cov}(f / g; \hat{\theta}^{(k)}) = [(\boldsymbol{I} - \boldsymbol{A})^t\boldsymbol{Q}_e^{-1}(\boldsymbol{I} - \boldsymbol{A}) + \boldsymbol{H}^t\boldsymbol{Q}_n^{-1}\boldsymbol{H}]^{-1} \tag{2.12}$$

And then, the conditional autocorrelation matrix $\hat{\boldsymbol{R}}_{\boldsymbol{ff}}$ and cross-correlation matrix $\hat{\boldsymbol{R}}_{\boldsymbol{fg}}$, which are defined by (2.13) and (2.14) are evaluated using $\hat{\boldsymbol{f}}$ and $\hat{\boldsymbol{V}}$.

$$\hat{\boldsymbol{R}}_{ff} = E(ff^t / g; \hat{\theta}) = \hat{\boldsymbol{V}} + \hat{\boldsymbol{f}}\hat{\boldsymbol{f}}' \tag{2.13}$$

$$\hat{\boldsymbol{R}}_{fg} = E(fg^t / g; \hat{\theta}) = \hat{\boldsymbol{f}}\boldsymbol{g}^t \tag{2.14}$$

Last, AR model coefficients $\hat{a}$ and model error $\hat{\sigma}_e^2$ are updated, and PSF values $\hat{h}$ and noise variance $\hat{\sigma}_n^2$ are estimated by (2.15) and (2.16).

$$\begin{aligned}&\hat{r}_{fg}(p,q)+\hat{r}_{fg}(-p,-q)-2\hat{r}_{fg}(0,0)-2\hat{r}_{ff}(p,q)+2\hat{r}_{ff}(0,0)\\&=2\sum_{m,n\in S_d^-}\hat{h}(m,n)\{\hat{r}_{ff}(p-m,q-n)+\hat{r}_{ff}(p+m,q+n)-2\hat{r}_{ff}(m,n)\\&-2\hat{r}_{ff}(p,q)+2\hat{r}_{ff}(0,0)\},\forall(p,q)\in S_d^-\end{aligned}\tag{2.15}$$

$$\hat{\sigma}_n^2=\frac{1}{N^2}\sum_{i,j=1}^{N}g(i,j)^2-\sum_{m,n\in S_d}\hat{h}(m,n)\hat{r}_{fg}(-m,-n)\tag{2.16}$$

Thus, $\hat{\theta}^{(1)}$ is obtained after the first iteration. The iteration process can be repeated many times until the reliable values of $\hat{\boldsymbol{f}}^{(k)}$ are derived.

## 2.3 Blind Image Deconvolution Based on Noise Variance Estimation

Blind image restoration methods can restore a blurred image without knowledge of the PSF, but they also have some defects, such as the large number of calculations and the large estimation error of the PSF [41]. The proposed method is to reduce the calculation and estimation error. In this Section, noise variance estimation and blur type reorganization are first introduced as image pretreatment. Then, according to the reorganized blur type, different approaches are implemented for estimating the image and blur model parameters.

### 2.3.1 Estimating the Noise Variance from the Observed Image

When taking the presence of noise into account, the estimation problem becomes more complicated because estimating the blur and noise parameters simultaneously may cause a large error. For the conventional EM method, the noise variance can be estimated using (2.16). We can see from (2.16) that in each iteration step, noise variance

is estimated on the basis of the estimated blur value which tends to cause a larger error. Therefore, the estimation error of noise variance $\hat{\sigma}_n^2$ becomes larger. In other words, the estimation of noise variance is influenced by blur estimation. Experimental results [32] show that the precise noise variance can only be obtained when the blur is of intermediate size and that a large estimation error results from blur a small or large size.

In order to improve this situation, we estimate the noise variance directly from the observed image. From the MA model (see (2.2)) we can see that image noise is independent of blur and is added after the image is blurred. Therefore, we can estimate the image noise from the observed image, assuming that the blurred image $h(x,y) * f(x,y)$ in (2.2) is the true image. Since the blurred image has less detail, it is easy to find smooth blocks; block-based methods can thus be used for estimating the noise variance. In this Section, the method of Amer and Dubois [52] is used to estimate the noise variance from the observed image. The method first selects intensity-homogeneous blocks in an image by rejecting blocks with a line structure using second-derivative masks to detect line structures. Then the global image noise variance is estimated from these selected homogeneous blocks. In this way, a stable noise variance value can be derived that is unrelated to the amount of blur. The estimated noise variance can be treated as a constant parameter during the next blur estimation process.

### 2.3.2 Estimating Blur Parameters for Different Blur Types

Many papers have proposed methods of parameter estimation for a particular blur type. However, they do not mention how to identify the blur type, which is also an important issue. Therefore, it is necessary to apply blur type reorganization as a pretreatment process. The three main types of blur are motion blur, defocus blur, and Gaussian blur, and their Fourier transforms have obvious differences. Thus, blur identification methods based on the Fourier transform [41], [56]-[58] can provide good results.

Blur estimation is much simpler when the blur type of the degraded image is classified. Different methods can be implemented on the basis of the different properties of the particular blur type.

#### 2.3.2.1 Linear Motion Blur

$$h(x,y;L,\phi)=\begin{cases}\dfrac{1}{C} & if\ \sqrt{x^2+y^2}\le\dfrac{L}{2}\ and\ \dfrac{y}{x}=\tan\phi\\ 0 & elsewhere\end{cases} \tag{2.17}$$

where $L$ is the length of motion and $\phi$ is the angle of motion direction. For linear motion blur, all the blur values are common and only determined by the length $L$. For the original EM method in [32], the blur parameter $L$ is estimated together with other ARMA model parameters, which tends to cause estimation error. In this Section, we propose a more efficient and straightforward method to obtain the precise blur values. Since the objective function (see (2.10)) is much more sensitive to the blur and noise parameters than the image model, and the blur pattern is discrete, we first compute the blur values under every blur size, and substitute them into the objective function, using the initial values of AR model coefficients. Then, these function values under every blur size are compared and the blur whose values lead to the lowest function value is chosen as the true blur. This iteration process can be started from the least blur size and stops when the minimum objective function value is obtained. For light blur, we can find the blur size within only several iterations; for heavy blur, the blur size can be obtained after dozens of iterations. At this stage, only the AR model parameters remain unknown, which are then estimated by the EM algorithm.

#### 2.3.2.2 Uniform Defocus Blur

$$h(x,y;R)=\begin{cases}\dfrac{1}{C} & if\ \sqrt{x^2+y^2}\le R\\ 0 & elsewhere\end{cases} \tag{2.18}$$

where each value of this blur is also a constant, thus it is similar to motion blur and its approximate 2-D lifting. Therefore, we can use the same method to find the true blur size.

### 2.3.2.3 Gaussian Blur

$$h(x,y;\sigma) = C\exp\left\{-\frac{x^2+y^2}{2\sigma_G^2}\right\} \tag{2.19}$$

where $\sigma_G^2$ is the Gaussian blur variance. For this kind of blur, it is still not necessary to identify the extent of the PSF because the blur size is directly derived from the identified value of $\sigma_G^2$ by truncation of the PSF at coefficients smaller than 0.1% of $h(0,0)$. The relationship between blur variance $\sigma_G^2$ and blur size is given in Table 2.1. We have only one blur parameter $\sigma_G^2$ to estimate. For this case, the EM algorithm is implemented to estimate the AR model parameters and $\sigma_G^2$ simultaneously.

### 2.3.2.4 Other Blur

For other unusual kinds of blur, no good method is available. We have to identify the blur size [59] first and then use nonparametric blur identification. Based on the symmetry pattern of blur, we must identify 4 unknown parameters for $3\times3$ blur and 12 parameters for $5\times5$ blur. For a larger size, the situation becomes more complicated.

Table 2.1 Relationship between Gaussian blur variance and blur size

| Gaussian blur variance | Blur size |
|---|---|
| 0.0724-0.2895 | 3×3 |
| 0.2895-0.6514 | 5×5 |
| 0.6514-1.1581 | 7×7 |
| 1.1581-1.8096 | 9×9 |

## 2.4 Experimental Results

In this Section, we report some experiments to validate the improved ML estimation algorithm based on noise variance estimation.

In order to reflect the advantages of the ARMA model, we use the texture image "leaf", which has low edge information, for the experiments (see Figure. 2.2). The image size is 128×128 pixels. Blur of different types and Gaussian noise with zero mean and a variance of 10 are added to the true image. First, we choose the block-based method [52] to estimate the noise variance and use the blur-type reorganization method based on the Fourier transform spectrum [41]. After we derive the noise variance and blur type, parameter estimation and image restoration for different blur types are implemented. In this paper, the initial conditions of the image model are chosen as

$a_{01}^{(0)} = 0.7$, $a_{10}^{(0)} = 0.7$, $a_{11}^{(0)} = -0.49$, $\sigma_e^{2(0)} = 100$.

As we know, selection of the initial values is a major problem. An accurate estimation result is only obtained when suitable initial conditions are selected. A large error appears when the initial values are not close to the true values for the original method. Our method, however, has improved this situation to some extent. Since in image restoration, the MA model values (blur and noise values) are more critical, they decide the restoration result directly. Since AR models are merely used to stabilize the inversion of PSFs, it is not necessary to have the exact AR model coefficients [32].

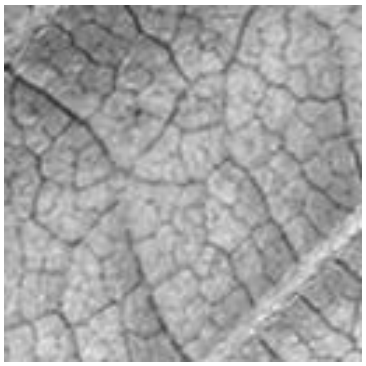

Figure 2.2 True "leaf" texture image

For the case of linear motion blur and uniform defocus blur, in our method, accurate values of blur and noise variance are identified in the first two steps; thus, a good restoration result can be obtained even for random AR initial conditions. Notably, for the case of Gaussian blur, the blur values must be estimated together with the AR model coefficients, but in our method the noise variance can be identified in advance, which can still lead to a better result than the original one.

### 2.4.1 Linear Motion Blur

For this blur, we choose an observed image with blur size 1×7. We substitute blur values for different blur sizes into the objective function, where the AR model coefficients are set as initial values, and find the minimum objective function value. The data are shown in Table 2.2, where the objective function value has been normalized to avoid the 'out of memory' problem.

We can see that the objective function value is extremely different for different blur sizes, and the minimum is obtained when the true size of 1×7 is used. Through this method, we can obtain the true blur size and precise blur values with no error. After this, the EM method is performed to estimate the remaining AR model coefficients (see Table 2.3). Then, the restored image is obtained by a least-squares filter [32] using all the estimated ARMA model coefficients (see Figure 2.3).

Table 2.2 Objective function values for different blur sizes

| Blur size | Blur value | Objective function value |
|---|---|---|
| 1×3 | 0.333 | 18.468 |
| 1×5 | 0.200 | 7.3511 |
| 1×7 | 0.143 | 1.0000 |
| 1×9 | 0.111 | 14057 |
| 1×11 | 0.091 | 15874 |

Table 2.3 Estimated AR model coefficients and noise variance

| | $a_{01}$ | $a_{10}$ | $a_{11}$ | $\sigma_e^2$ | $\sigma_n^2$ |
|---|---|---|---|---|---|
| **True value** | 0.652 | 0.657 | -0.310 | 136.84 | 10 |
| **Estimated value** | 0.704 | 0.630 | -0.303 | 142.05 | 10.207 |

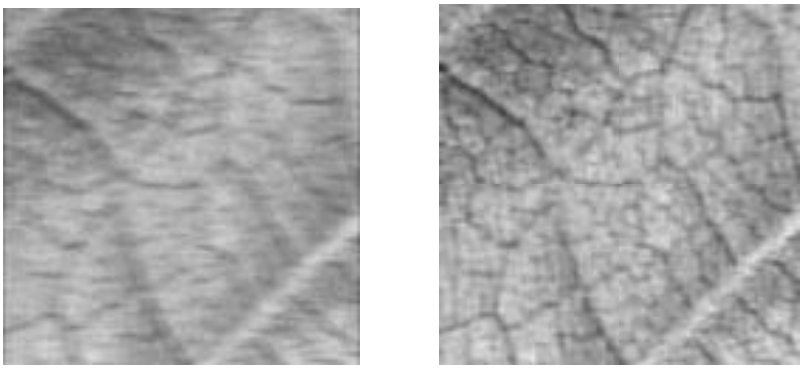

(a) (b)

Figure 2.3 Restoration result of motion-blurred noisy image
(a) motion-blurred noisy image (blur size 1×7)
(b) restored image (ISNR = 5.4832 dB)

### 2.4.2 Uniform Defocus Blur

Uniform defocus blur is similar to motion blur and its approximate 2-D lifting. Therefore, we can use the same method as that in 2.5.1 to find the true blur values. The imposed blur size is 5×5 with blur radius *R* 2.236 (see (2.20)).

$$h = \begin{bmatrix} 0 & 0.0476 & 0.0476 & 0.0476 & 0 \\ 0.0476 & 0.0476 & 0.0476 & 0.0476 & 0.0476 \\ 0.0476 & 0.0476 & 0.0476 & 0.0476 & 0.0476 \\ 0.0476 & 0.0476 & 0.0476 & 0.0476 & 0.0476 \\ 0 & 0.0476 & 0.0476 & 0.0476 & 0 \end{bmatrix} \tag{2.20}$$

The obtained objective function values for different blur radius and the image restored from the imposed blur are shown in Table 2.4 and Figure 2.4, respectively.

Table 2.4 Objective function values for different blur sizes

| Blur size | Blur radius | Blur value | Objective function value |
|---|---|---|---|
| 3×3 | 1.414 | 0.111 | 11.538 |
| 5×5 | 2.000 | 0.077 | 55.096 |
| 5×5 | 2.236 | 0.0476 | 1.0000 |
| 5×5 | 2.828 | 0.040 | 105.44 |
| 7×7 | 3.000 | 0.0345 | 32.445 |

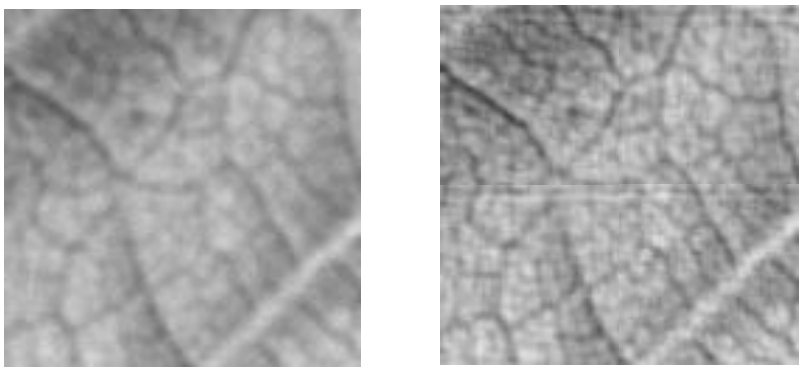

(a) (b)

Figure 2.4 Restoration result of defocus-blurred noisy image
(a) defocus-blurred noisy image (blurred by (2.20))
(b) restored image (ISNR = 4.5687 dB)

### 2.4.3 Gaussian Blur

For Gaussian blur, we use the EM method to estimate the AR model and MA model coefficients simultaneously. In order to verify our method, we use different Gaussian blur variances and compare the estimated noise variance between the original method [33] and our method. The initial value of blur variance is set as 0.5.

First, we repeat the experiments of [32]. Whereas the results in [48] are based on quite low noise, we added larger noise with a variance of 10 to obtain a better comparison (See Table 2.5).

It is observed that for the original method, the estimated noise variance depends on the blur size. From the experimental result of [32], when the blur variance is 0.2 or 1.0, a large estimation error of the noise variance is obtained. The true noise variance is 10, but the estimated values of noise variance for the two blur variances are 12.5698 and 8.7308, respectively. Precise values can only be obtained for the case of intermediate blur sizes and a large error is obtained for the case of small and large blur sizes. However, from the results obtained by our method (see Table 2.6), the estimated noise values are stable and fluctuate around the true value for every blur size. In other words, the estimated noise variance is independent of the blur size. Precise results for the noise variance lead to better image restoration results. Here, we restore the blurred image with a blur variance

Table 2.5 Estimated Gaussian blur and noise variances using original method

| Blur size | True blur variance | Estimated blur variance | Estimated noise variance |
|---|---|---|---|
| 3×3 | 0.2 | 0.2088 | 12.5698 |
| 5×5 | 0.3 | 0.2651 | 12.9831 |
| 5×5 | 0.4 | 0.3704 | 11.5174 |
| 5×5 | 0.5 | 0.4759 | 11.6016 |
| 5×5 | 0.6 | 0.5700 | 10.5001 |
| 7×7 | 0.7 | 0.7114 | 10.3204 |
| 7×7 | 0.8 | 0.7939 | 9.5884 |
| 7×7 | 0.9 | 0.8631 | 9.2956 |
| 7×7 | 1.0 | 1.0126 | 8.7308 |

Table 2.6 Estimated Gaussian blur and noise variances using our method

| Blur size | True blur variance | Estimated blur variance | Estimated noise variance |
|---|---|---|---|
| 3×3 | 0.2 | 0.2075 | 10.2831 |
| 5×5 | 0.3 | 0.2654 | 10.2492 |
| 5×5 | 0.4 | 0.3895 | 9.5736 |
| 5×5 | 0.5 | 0.4989 | 10.6274 |
| 5×5 | 0.6 | 0.5820 | 10.1970 |
| 7×7 | 0.7 | 0.6897 | 9.9375 |
| 7×7 | 0.8 | 0.7977 | 9.8048 |
| 7×7 | 0.9 | 0.9055 | 10.0382 |
| 7×7 | 1.0 | 1.0160 | 9.8943 |

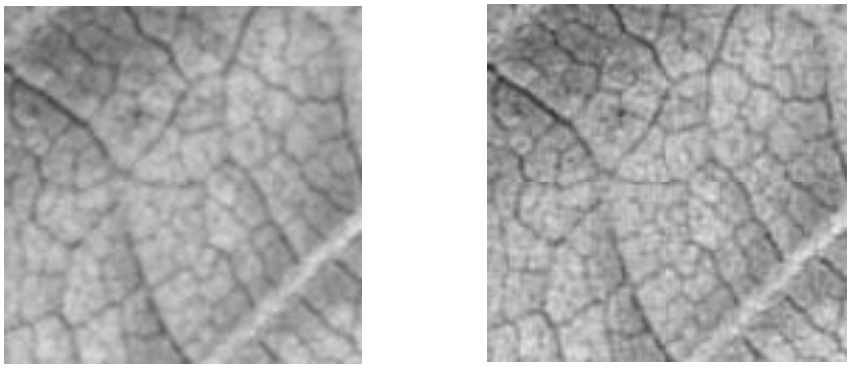

(a) (b)

Figure 2.5 Restoration result of Gaussian blurred noisy image
(a) Gaussian blurred noisy image (blur variance 0.6)
(b) restored image (ISNR = 4.4732 dB)

of 0.6 as an example (see Figure 2.5).

### 2.4.4 Other Blur

As an example of another type of blur, we choose an unusual type of 3×3 blur. The blur parameters are

$$h = \begin{bmatrix} 0.0540 & 0.1244 & 0.0540 \\ 0.1244 & 0.2864 & 0.1244 \\ 0.0540 & 0.1244 & 0.0540 \end{bmatrix} \tag{2.21}$$

Using the symmetry property of blur, four free coefficients are needed for this blur. The total number of free parameters in $\theta$ is therefore equal to 9. The identified results of blur and noise are expressed as

$$\hat{h} = \begin{bmatrix} 0.0746 & 0.1244 & 0.0539 \\ 0.1240 & 0.3208 & 0.1240 \\ 0.0539 & 0.1244 & 0.0746 \end{bmatrix} \tag{2.22}$$

$$\hat{\sigma}_n^2 = 10.155$$

and restoration result is shown in Figure 2.6.

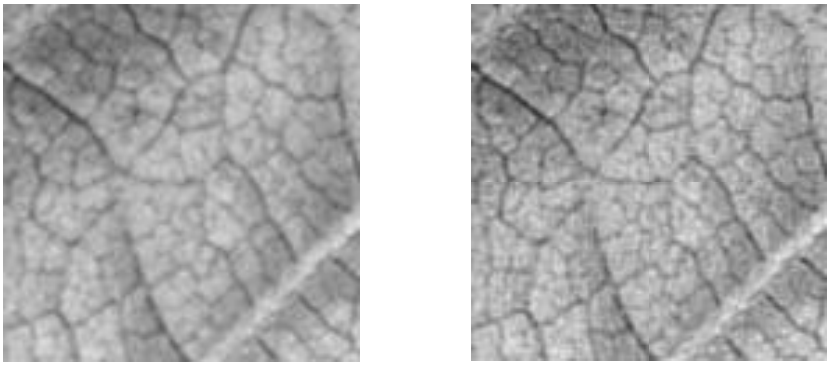

(a) (b)

Figure 2.6 Restoration result of unknown blurred noisy image
(a) blurred noisy image (blurred by (2.21))
(b) restored image (ISNR = 4.5301 dB)

## 2.5 Summary

We have described a novel blind image restoration method based on noise variance estimation. A noise variance estimation method and blur type reorganization process are implemented first. Then, according to the reorganized blur type, different methods are used to obtain the parameter values. Images are restored by the least-squares filter using the estimated parameters in each iteration step. Experiments with observed images suffering from three common types of blur and an unknown blur were performed to validate our method.

Chapter 3

# 3 Improved Structure-Based Gaussian Noise Variance Estimation Method

Noise can significantly impact the effectiveness of digital image processing. In this Chapter, an improved structure-based Gaussian noise variance estimation algorithm is presented. This method first separates the image into blocks and calculates homogeneity measures of every block through the proposed masks, taking the image structure into account. Then, the most homogeneous blocks are selected using a new threshold. Finally, pixel value variances of all selected blocks are averaged to estimate the global noise variance for one image. Comparative experiments with a variety of images using the proposed method and original structure-oriented method are described, and the experimental results show that the proposed method is feasible and effective, especially for good-quality images.

## 3.1 Related Works

Image noise comprises random variations in brightness or color, and can be produced by the sensor and circuitry of a scanner or camera. When information on such noise becomes available, an image processing algorithm, such as filtering [60]-[62], edge detection [63]-[65], image segmentation [66]-[68], or image compression [69]-[71], can be adapted to the amount of noise to provide significantly improved performance [52]. Therefore, noise variance estimation has been a fundamental and important task in image processing systems.

Noise can be estimated within one image or between multiple images. In this Chapter, we only focus on the estimation from one image, which requires less memory and less computational demand. The one-image estimation methods can, in general, be classified into the following two types.

(a) Filtering-based approach, in which the image is first filtered to suppress the influence of the original image, and then the variance of the filtered image is assumed to be the noise variance. Rank et al. [72] first filtered a noisy image using a horizontal and vertical difference operator, and then obtained the desired estimation value using the histogram of local signal variances. Pei et al. [53] processed a noisy image using a group of high-pass digital filters constructed of several finite difference operators with different orders. A low-pass filter such as an averaging filter, has also been used to preprocess images (smooth-based approach). The filtering approach requires much computation and encounters difficulties with images having fine texture.

(b) Block-based approach, in which the variance over a set of blocks of the image is calculated and the average of the smallest block variances is taken as an estimate of the global noise variance [73]. Liu et al. [74] presented a fast and efficient noise variance estimation algorithm through a window and the corresponding operation of computing variance. Shin et al. [75] computed the standard deviation of selected blocks from the difference between the noisy input and the filtered input. The block-based approach is several times faster than the filtering-based approach, but the main difficulties are how to select the threshold for the variance averaging process, and that the smallest variances do not always lead to a good homogeneity measure.

Recently, a novel structure-oriented noise variance method has been proposed [52]. This method is also based on blocks, but it takes the image structure into account and uses a measure other than the variance to determine if a block is homogeneous. This technique gives more reliable estimates than the block-based methods in their basic form, but tends to overestimate the amount of noise, especially in the case of good-quality images. In this study, this structure-oriented method is improved by using a new homogeneity measure and a different threshold. The overestimation problem with good-quality images has also been solved.

Most noise variance estimation methods assume that the noise signal is additive Gaussian white noise. Thus, in this Chapter, we also use this noise model, which is represented by blur and noise are expressed as

$$g(x,y) = f(x,y) + n(x,y) \tag{3.1}$$

where $f(x,y)$ is the original image signal, $g(x,y)$ is the noisy image signal, and $n(x,y)$ is the noise signal at coordinate $(x,y)$. Generally, an image is defined as a $X \times Y$ matrix, in which each element is a pixel value between 0 and 255.

The structure of this Chapter is as follows. In Section 3.1, previous works on this topic are described. The new masks used for homogeneity measurement are first discussed, and the proposed threshold for variance averaging is then presented in Section 3.2. Experimental results for images with homogeneous areas and fine textures are shown in Section 3.3, and a summary is given in Section 3.4.

## 3.2 Proposed Image Noise Variance Estimation Method

In order to alleviate the overestimation of the amount of noise in [52], the proposed method in this Section presents new masks for homogeneity measurement and a more accurate threshold for the averaging process.

### 3.2.1 Homogeneity Measure

As described in Section 2.1, the observed image suffers from additive noise. When calculating the noise variance directly from the degraded image, a large error arises owing to the structure of the true image, which leads to the extra variance. Therefore, if we estimate the noise variance from the relatively homogeneous areas in an image, the result is reliable. As we know, an image usually comprises homogeneous areas and sharp areas. Thus, it can be divided into many blocks, of which only homogeneous ones are used for noise variance estimation.

In [52] the authors showed that the dividing pattern of 5×5 blocks is a good compromise between efficiency and effectiveness. Thus, the same dividing pattern is used in this Section. For example, an image of 256 × 256 size can be separated into 51 × 51 blocks. Then the homogeneity for every block is checked. In [52], a uniformity

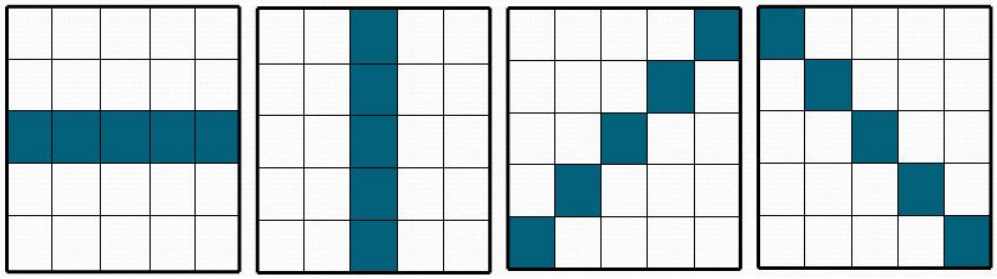

mask-1 mask-2 mask-3 mask-4

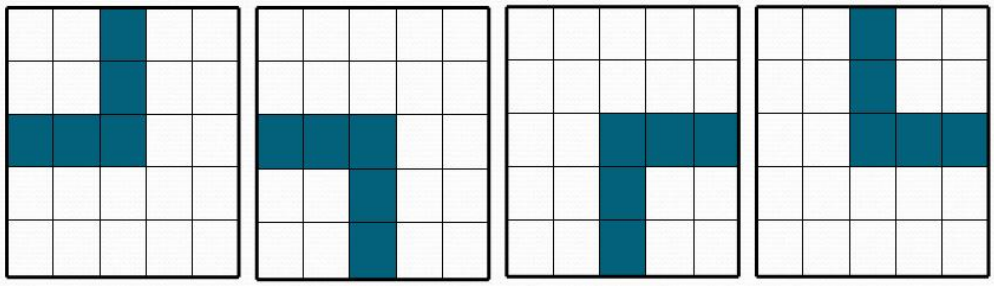

mask-5 mask-6 mask-7 mask-8

Figure 3.1 The homogeneity analyzer for $5\times5$ blocks

analyzer based on 8 masks and high-pass operators was used to measure homogeneity, as is shown in Figure 3.1. In Figure 3.1, the colored pixels indicate the eight different directions for homogeneity measurement. The first four directions respond well for line, step, and shoulder edges, and the last four corner directions are used for detecting the center edges. For each block, high-pass operators are applied on the colored pixels along the eight directions. The coefficients of the high-pass operators are

$$\{-1,-1,4,-1,-1\} \tag{3.2}$$

Then, eight homogeneity values along the eight directions are calculated, i.e.,

$$H_j = -f(i-2) - f(i-1) + 4 \cdot f(i) - f(i+1) - f(i+2) \qquad j = 1,2,\cdots 8 \tag{3.3}$$

where $i$ is the coordinate of the center pixel along one direction, $f$ is the pixel value, and $H_j$ is the homogeneity value for one direction. Lastly, the absolute values of all eight quantities are added to give the homogeneity value for one block.

$$H_m = |H_1| + |H_2| + \cdots + |H_8| \tag{3.4}$$

For a homogeneous block, the homogeneity measure for a certain direction $H_j$ is close to 0, and the global homogeneity measure $H_m$ is low.

The masks described in [52] lead to reliable results; however, there are still eight pixels remaining unchecked within one block. Combining all the eight masks into one block, we have the masks shown in Figure 3.2. In Figure 3.2, we can see that eight pixels are not covered by the eight masks, which is a considerable problem. It causes difficulties when the pixel values undergo extreme changes in uncovered places. Four novel masks are proposed in this Section, which are shown in Figure 3.3. The four proposed directions are used to compensate for the eight noncovered pixels.

The four proposed masks can detect the curved edges around the border in one block, which cannot be achieved using the previous eight masks. As is well known, all of the masks are used to detect the edge information along a certain direction. As discussed concerning the original method, masks 1-4 can detect the line, step, and shoulder edges, and masks 5-8 can detect the center edges. Similarly, the proposed masks 9-12 can detect the curved edges. Thus, the proposed masks can compensate for not only the unchecked pixels but also the unchecked curved edges and lead to better homogeneity

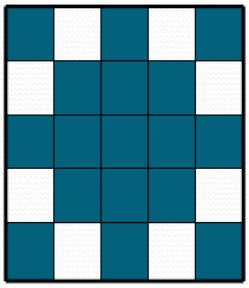

Figure 3.2 Combined mask of all eight directions

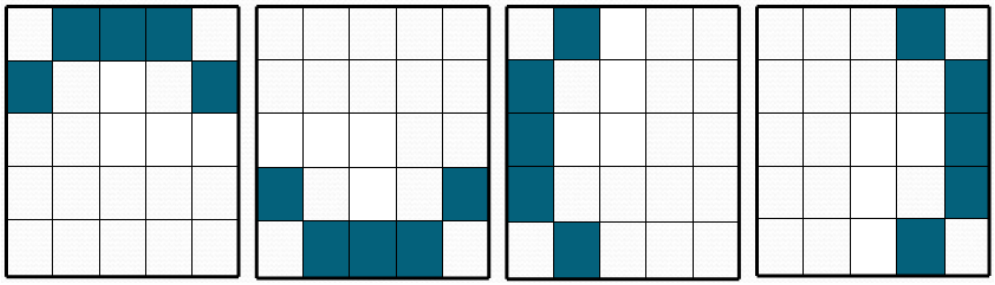

mask-9 mask-10 mask-11 mask-12

Figure 3.3 Four proposed compensation masks

measurement.

Here, we note that the ‘reference pixels’ (in the center of one direction multiplied with element {4}) for the new masks differ from those for the conventional masks. This is because the idea for edge detection is different. For the proposed method, we do not set the reference pixels because we consider one block to be a whole target. Thus, the homogeneity value of the proposed method is not for the center pixel but for the whole block. We can detect all of the possible edges using the eight original and four proposed masks. We need not overlap these blocks, unlike in [52]. (For example, the proposed method uses only 51×51 blocks for a 256×256 image ( 256/5 = 51 ) ). In other words, we use fewer blocks but obtain more accurate estimation results. Therefore, a more reliable result can be achieved in this way without problems.

In this work, the original eight masks and the four proposed masks are all used for computing the homogeneity value. Thus, the global homogeneity value for one block is

the absolute sum of those for all twelve directions.

### 3.2.2 Threshold for Variance Averaging

Using the above twelve masks and high-pass operators, homogeneity values for every block are calculated. However, only the variances of the most homogeneous blocks, which can be taken to represent noise in the whole image, are used for the variance averaging process. Thus, an accurate threshold for rejecting the blocks with a large estimation error is needed. Amer and Dubois [52] used the following equation:

$$\left| PSNR_{B_r} - PSNR_{B_{ij}} \right| < t_{PSNR} \tag{3.5}$$

or

$$PSNR_{B_r} - t_{PSNR} < PSNR_{B_{ij}} < PSNR_{B_r} + t_{PSNR} \tag{3.6}$$

where PSNR (dB) is a standard criterion for the objective measurement of image noise, and the transform between PSNR and variance is defined by

$$PSNR = 10 \cdot \log_{10} \frac{255^2}{\sigma^2} \tag{3.7}$$

In (3.5) and (3.6), $PSNR_{B_r}$ is the reference PSNR, which is chosen as the median of the PSNR of the three most homogeneous blocks. Here, $PSNR_{B_r}$ is assumed to be a rough noise variance estimation of the whole image. $PSNR_{B_{ij}}$ is the PSNR of a certain block, and $PSNR_{B_r}$ is the threshold set to 3 dB. We must use this threshold to select the blocks with similar variance to $t_{PSNR}$.

However, the function of PSNR in (3.7) changes exponentially, which causes

different selection ranges between the two sides of $PSNR_{B_r}$ in (3.6). Here the selection range is from $PSNR_{B_r} - t_{PSNR}$ to $PSNR_{B_r} + t_{PSNR}$. This tends to cause the overestimation of noise variance. For example, we set the reference PSNR, $PSNR_{Br}$, to 30 dB; then we can obtain the selection range of 27-33 dB using (3.5) or (3.6). Then we select the blocks with PSNR of 27-33 dB and average the pixel variance of these blocks. As PSNR of 27-33 dB indicates a variance of 33-130, we obtain the averaging result of about 81.5. However, we know that the reference variance is 65 ($PSNR_{Br}$ 30); thus, we have overestimated the noise variance. As the reference PSNR increases, the overestimation problem will become more critical. This is also the reason why the algorithm in [52] has difficulties with good-quality images.

In this paper, a new threshold is proposed:

$$\begin{aligned} &\left|\sigma_{B_r}^2 - \sigma_{B_{ij}}^2\right| < t_D \\ &t_D = \left|\sigma_{B_r}^2 - \sigma_{B_{\min}}^2\right| \end{aligned} \tag{3.8}$$

or

$$\sigma_{B_r}^2 - t_D < \sigma_{B_{ij}}^2 < \sigma_{B_r}^2 + t_D \tag{3.9}$$

where $\sigma_{B_r}^2$ is the reference variance, which is the median of the variances of the three most homogeneous blocks, $\sigma_{B_{ij}}^2$ is the variance of a certain block, and $t_D$ is the proposed threshold, which is chosen as the difference between the reference variance and the minimum variance. This new equation for block selection is similar to (3.5) (or (3.6)) but it can improve the overestimation situation because it has the same selection ranges between the two sides of $\sigma_{B_{ij}}^2$ in (3.9). Also, the new variable threshold is reliable over a wide range of noise conditions.

After selecting the homogeneous blocks using (3.8), the variances of the selected

blocks are averaged to give the estimated global variance.

## 3.3 Experimental Results

In this Section, ten images of 256 × 256 size (see Figure 3.4) are used to validate the proposed method for noise variance estimation. The first five images have some homogeneous areas and the latter five images have fine textures. Comparisons of masks and thresholds between the proposed method and the original method addressed in [52] are reported.

To evaluate the performance of the proposed algorithm, the averages of estimation results are first calculated to indicate the accuracy of the estimation (3.10), and then, the averages of estimation errors are computed to check the stability (3.11) of every noise level:

(a) (b)

(c)

(d)

(e)

(f)

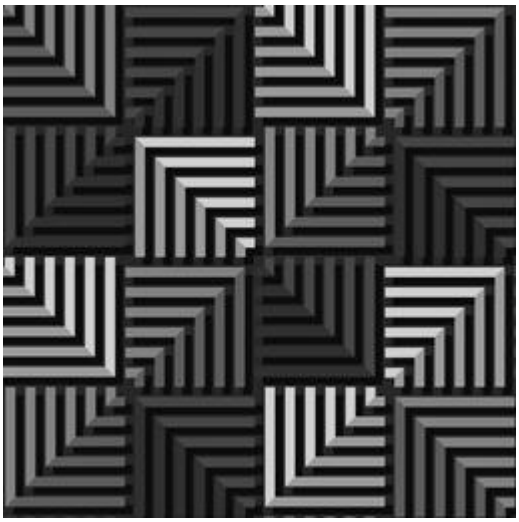

(g)

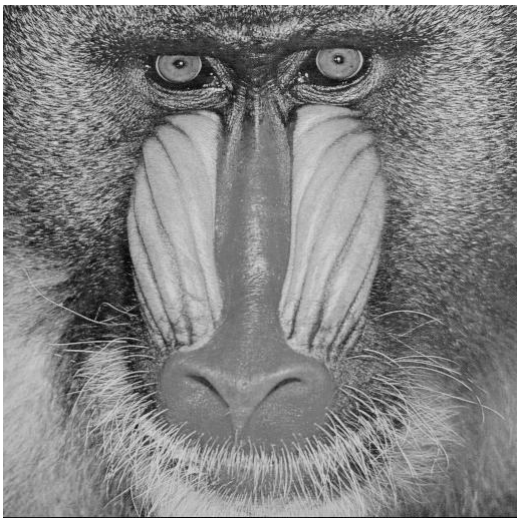

(h)

(i)

(j)

Figure 3.4 Images used for experiments: (a) Uniform, (b) Cameraman, (c) Boat, (d) Couple, (e) Lena, (f) Cabinet, (g) Synthetic, (h) Baboon, (i) Bridge, and (j) Arial

$$\mu_{R_{PSNR}} = \frac{\sum_{N}\sum_{M} R_{PSNR}}{N \cdot M} \tag{3.10}$$

where $R_{PSNR}$ is the noise variance estimation result of a certain image in one estimation, $\mu_{R_{PSNR}}$ is the average of the estimation results, $M$ is the number of estimations, and $N$ is the number of images.

$$\mu_{E_{PSNR}} = \frac{\sum_{N}\sum_{M} \left| R_{PSNR} - T_{PSNR} \right|}{N \cdot M} \tag{3.11}$$

Here, $T_{PSNR}$ is the true PSNR and $\mu_{E_{PSNR}}$ is the average estimation error. In this experiment, one hundred repetitions of estimation are processed for every noise level, thus $N$ is 10 and $M$ is 100.

### 3.3.1 Comparison of Masks

First, comparison results when only the masks were changed are shown in Figure 3.5. The black line ‘true’ corresponds to the true data of the PSNR of noise, that is, estimation without error. This is used to describe the distance between the estimated results and true data. As shown in Figure 3.5, the estimated results for the proposed masks outperform the original ones for all noise levels and the estimation at 20 dB is similar to the true data (Figure 3.5(a)). The estimation error is lower for most noise levels other than the similar result at 20 dB (Figure 3.5(b)).

### 3.3.2 Comparison of Threshold

In Figure 3.6, the results of an evaluation of the proposed threshold are given. The comparison suggests better performance with the proposed threshold. It alleviates the overestimation problem at every noise level (Figure 3.6(a)). For 20 dB and 25 dB, the estimation results are similar to the true data.

### 3.3.3 Combining the masks and threshold

Lastly, for a more reliable evaluation, the proposed masks and threshold are combined. As can be seen in Figure 3.7, the estimated results and estimation error are improved more significantly than in Figures 3.5 and 3.6. Note that the noise variance between 20 dB and 25 dB tends to be under-estimated but the accuracy is still similar to the original

accuracy. Figure 3.7(b) reveals that the estimation error of the proposed method is higher at 20 dB. This is reasonable since 20 dB is a very high noise level and the variance of noise is much larger than that of the image structures. In this case, the influence of the image structure on noise variance estimation is not significant. Thus, the proposed masks with greater accuracy of edge detection do not provide an improved performance. At the same time, the new threshold tends to provide a smaller selection range from the simulation results. However, in the case of 20 dB, the noise between different blocks exhibits much more deviation than in the cases of other noise levels, whereby a larger selection range is needed for good stability of estimation.

### 3.3.4 Comparison of Images with Homogeneous Areas and Images with Fine Texture

In order to check the different effects of the proposed method on two different kinds of images, separate results are shown in Figures 3.8 and 3.9. As can be seen, since the proposed method is more sensitive to the image structure and more effective in detecting the edge information, the results for fine texture images, Figures 3.4 (f)-(j), for every noise level are outstanding compared with the original accuracy (Figure 3.9). For images (a)-(e) in Figure 3.4, with homogeneous areas, the proposed method also provides a significant improvement (Figure 3.8) with the estimation error being higher at 20 dB, similar to the case of Figure 3.7(b). The reason for this is as described in Section 3.3.3; the performance of the proposed method is poor at extremely high noise levels for images with homogeneous areas.

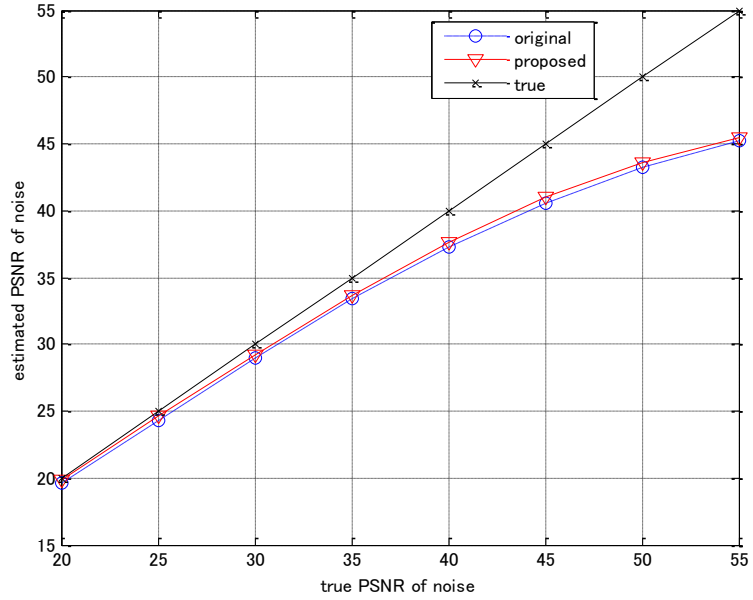


(a)

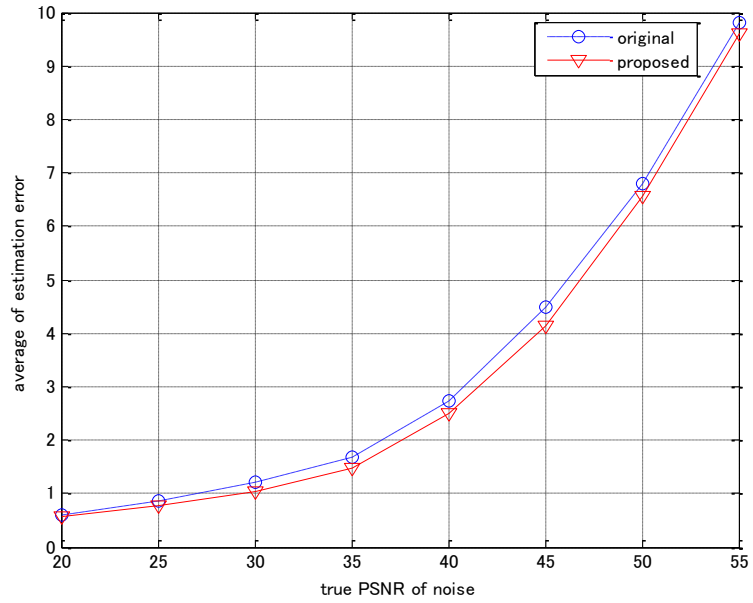


(b)

Figure 3.5　Comparison of original masks and proposed masks: (a) Average of estimation results, (b) Average of estimation error

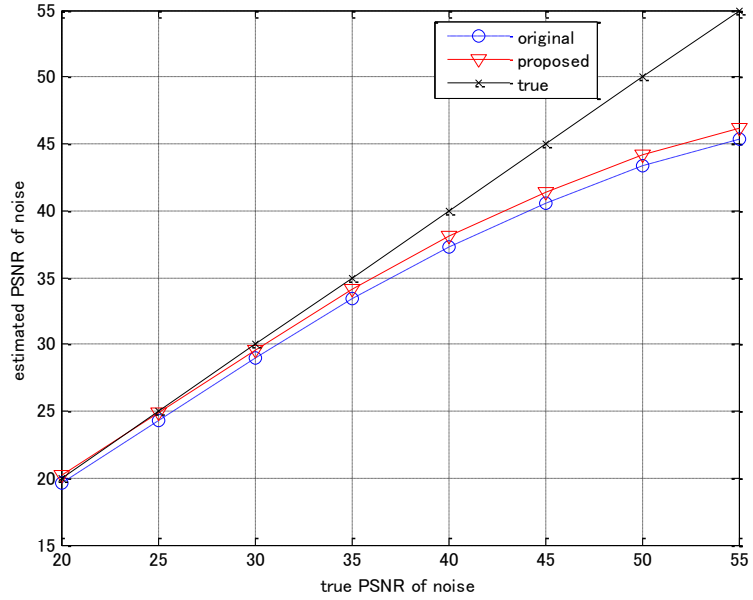


(a)

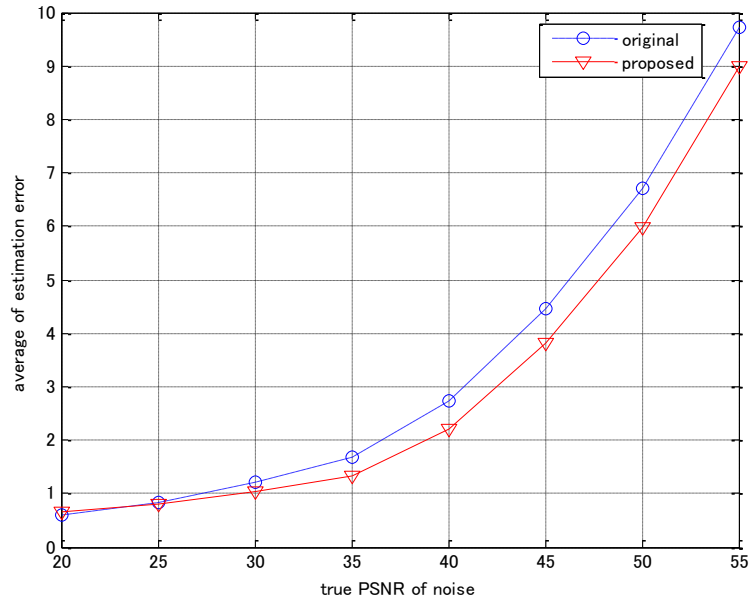


(b)

Figure 3.6　Comparison of original threshold and proposed threshold: (a) Average of estimation results, (b) Average of estimation error

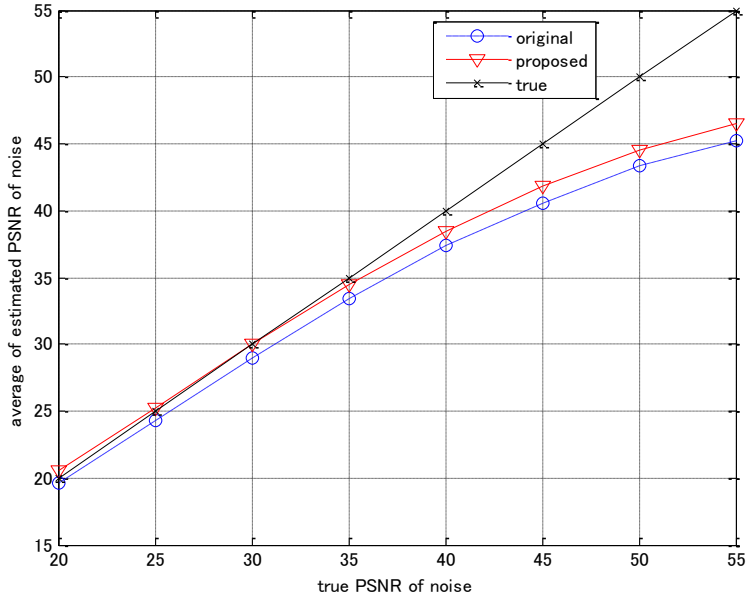


(a)

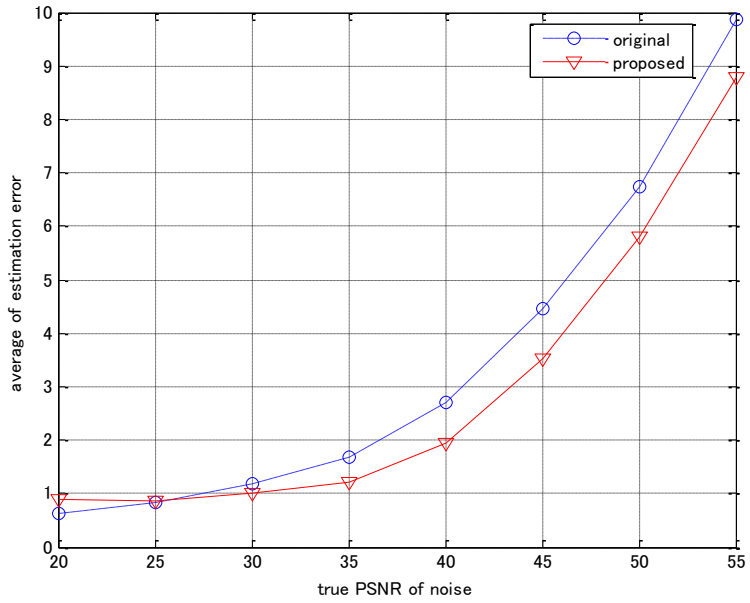


(b)

Figure 3.7 Results for combining the masks and threshold:
(a) Average of estimation results, (b) Average of estimation error

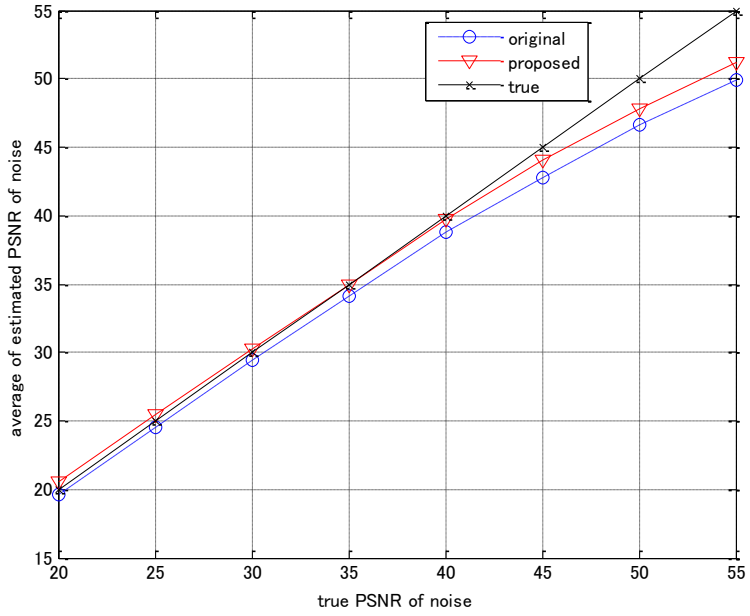


(a)

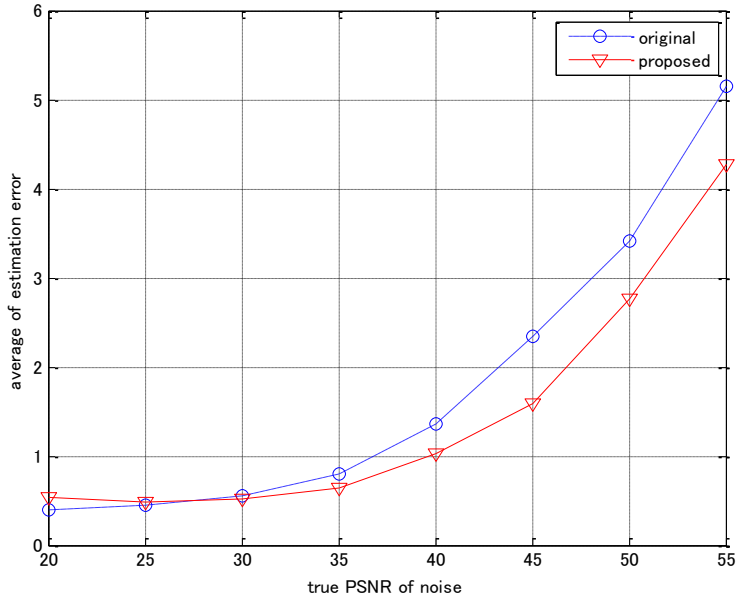


(b)

Figure 3.8 Results for images (a)-(e) in Figure 3.4, combining the masks and threshold: (a) Average of estimation results, (b) Average of estimation error

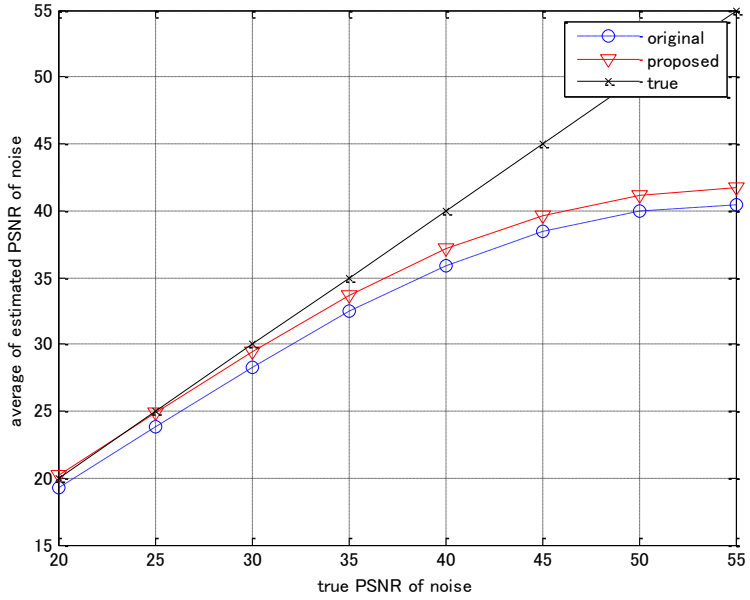


(a)

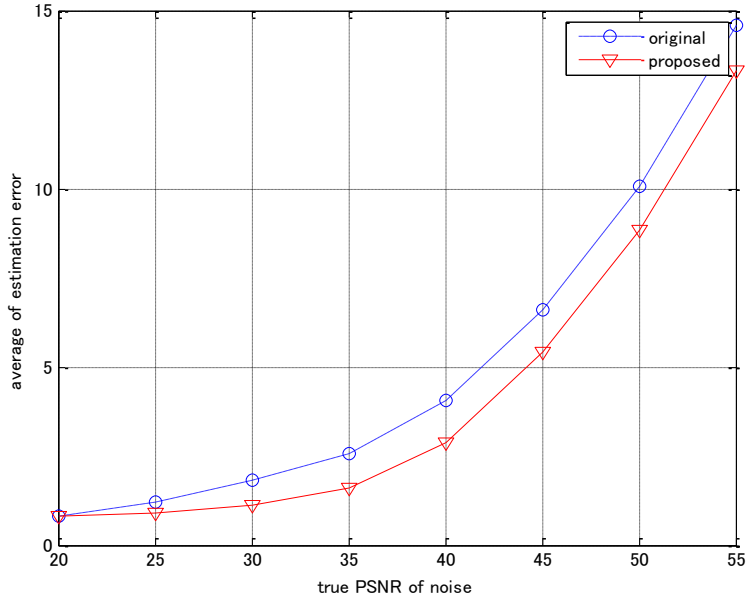


(b)

Figure 3.9 Results for images (f)-(j) in Figure 3.4, combining the masks and threshold: (a) Average of estimation results, (b) Average of estimation error

## 3.4 Summary

We proposed a novel and reliable method for noise variance estimation in noisy images. This method requires a 5×5 mask and averages the noise variances of homogeneous image blocks, where only blocks showing similar homogeneities are included in the averaging process. New masks covering every pixel in one block and a variable threshold for the variance averaging process were proposed. The proposed method alleviates the overestimation problem significantly and reveals better robustness for estimation at most noise levels. Experiments with images including homogeneous areas and fine textures were described. Experimental results demonstrated that our method is feasible and effective for noise variance estimation, especially for good-quality images.

Chapter 4

# 4 Difference Eigenvalue Based Gaussian Noise Variance Estimation Method

Noise can significantly impact the effectiveness of digital image processing. In this Chapter, a difference eigenvalue based noise variance estimation algorithm is presented. This method first calculates the difference eigenvalue edge indicator values of every pixel in an image. Then, according to the indicator values, proper threshold is set to determine that a pixel is homogeneous or texture pixel. Next, the image is separate into many blocks and only the blocks including only homogeneous blocks are selected for the next averaging step. Last, pixel value variances of every homogeneous block are averaged leading to the global estimation result.

## 4.1 Related Works

Digital images usually suffer from added noise from various sources, such as acquisition, compression, transmission and reconstruction. When information on such noise becomes available, an image processing algorithm, such as filtering [60]-[62], edge detection [63]-[65], image segmentation [66]-[68], or image compression [69]-[71], can be adapted to the amount of noise to provide significantly improved performance [52]. Therefore, noise variance estimation has been a fundamental and important task in image processing systems.

Many noise variance estimation methods have been developed over years. Among them, Amer et al. [52] proposed a structure-oriented white-noise variance estimation algorithm. This method finds intensity-homogeneous blocks using a new structure analyzer for rejecting blocks with structure. However, it tends to overestimate the noise level for the case of good-quality images. Liu et al. [76] proposed an iteration method to estimate the noise level using principal component analysis if an image comprises only weak textured patches, which are selected using the gradients of the patches and their statistics. However, as well known, for this iteration method, an initial noise variance is needed and it can only be determined using the degraded image first. Zhai et al. [77] developed a framework for estimating noises of natural images using two important properties of natural images statistics: high kurtosis and scale invariance. They proposed an objective function for noise estimation assuming that skewness and kurtosis can be considered as a constant in certain transform domains such as discrete cosine transform. However, this property is not quite proper for some images whose kurtosis has some changes through different frequency.

Recently, a novel image noise removal method based on difference eigenvalue has been proposed [78]. It showed that the value of the difference eigenvalue edge indicator changes obviously corresponding to the homogeneous blocks or the fine texture blocks. Thus, in this Chapter, we focus on the noise variance estimation using this difference eigenvalue edge indicator. We determine a proper threshold to this filter and select the homogeneous blocks which are used for the global noise estimation.

The structure of this Chapter is as follows. In Section 4.1, previous works on this topic have been described. The Hessian matrix and difference eigenvalue edge indicator are first discussed, and then the proposed threshold for selection of homogeneous blocks is then presented in Section 4.2. Experimental results for images with fine textures are shown in Section 4.3, and a summary is given in Section 4.4.

## 4.2 Proposed Image Noise Variance Estimation Method

In order to estimate the image noise variance using the difference eigenvalue based edge indicator in [78], a new threshold for the selection of homogeneous blocks is

proposed in the proposed method.

### 4.2.1 Hessian Matrix

The difference eigenvalue edge indicator is calculated from the Hessian matrix of second-order derivatives of an image. And it has been shown that image details can be better revealed by second-order operators [79]-[81].

For a certain pixel value in one image, $f(x, y)$, the Hessian matrix is defined as

$$H = \begin{bmatrix} f_{xx} & f_{xy} \\ f_{xy} & f_{yy} \end{bmatrix} \tag{4.1}$$

where $f_{xx}, f_{xy}, f_{yy}$ is the second-order derivatives of difference directions which can be calculated by

$$\begin{aligned} f_{xx} &= f_x(x+1, y) - f_x(x, y) \\ &= f(x+2, y) - f(x+1, y) - [f(x+1, y) - f(x, y)] \\ &= f(x+2, y) - 2f(x+1, y) + f(x, y) \end{aligned} \tag{4.2}$$

Similarly,

$$f_{xy} = f(x+1, y+1) - f(x+1, y) - f(x, y+1) + f(x, y) \tag{4.3}$$

$$f_{yy} = f(x, y+2) - 2f(x, y+1) + f(x, y) \tag{4.4}$$

Matrix *H* is positive semidefinite with two eigenvalues $\lambda_1$ and $\lambda_2$, which is

$$\lambda_1 = \frac{1}{2}\left[(f_{xx} + f_{yy}) + \sqrt{(f_{xx} - f_{yy})^2 + 4f_{xy}^2}\right] \tag{4.5}$$

$$\lambda_2 = \frac{1}{2}\left[(f_{xx} + f_{yy}) - \sqrt{(f_{xx} - f_{yy})^2 + 4f_{xy}^2}\right] \tag{4.6}$$

where $\lambda_1$ corresponds to the maximum local variation at a pixel and $\lambda_2$ corresponds to the minimum local variation.

### 4.2.2 Difference Eigenvalue Edge Indicator

Using the calculated eigenvalues $\lambda_1$ and $\lambda_2$, the difference eigenvalue edge indicator is defined as

$$I(f) = (\lambda_1 - \lambda_2)\lambda_1 w(f(x,y)) \tag{4.7}$$

where $w(f(x,y))$ is weighting parameter, which is used to achieve a balance between detail enhancement and noise suppression, defined by

$$w(f(x,y)) = \theta \frac{\sigma^2(x,y) - \min(\sigma^2)}{\max(\sigma^2) - \min(\sigma^2)} \tag{4.8}$$

$\sigma^2$ is the average gray-level variance of $f(x,y)$, which can be calculated from its 3×3 neighborhood

$$\sigma^2(x,y) = \frac{1}{3^2}\sum_{i=-1}^{1}\sum_{i=-1}^{1}[f(x+i, y+j) - f(x,y)] \tag{4.9}$$

Among the nine values, the maximum and minimum values are defined as $\max(\sigma^2)$ and $\min(\sigma^2)$, respectively. $\theta$ is a constant.

In edge areas, $\lambda_1$ is large and $\lambda_2$ is small, thus $\lambda_1 - \lambda_2$ is large, giving a large $I(f)$; while in homogeneous areas, the values of $\lambda_1$ and $\lambda_2$ are both small and similar, thus giving a small $I(f)$. As can be seen from the behavior analysis of the difference eigenvalue edge indicator, edge information and homogeneous area could be distinguished effectively.

### 4.2.3 Threshold for Selection of Homogeneous Blocks

Based on the behavior analysis of the difference eigenvalue edge indicator, a threshold is further needed which is used to distinguish that where is homogeneous and where is edge information. Experiment results show that the value 20 is a good choice, especially for the fine texture images. Thus, the pixels, of which the indicator value $I(f)$ is larger than 20, are considered as the edge information (see (4.10)).

$$\begin{cases} I(f) > 20, \text{ rejected} \\ I(f) \le 20, \text{selected} \end{cases} \tag{4.10}$$

For the general noise estimation process, we first separate an image into many overlapping blocks with 5×5 pixels (For example, for an image with the size 256×256, there are 252×252 overlapping blocks with 5×5 pixels.), and then using the proposed threshold, only the blocks without edge information are selected. Last, variances of the pixel values in the selected blocks are averaged to estimate the global noise variance (see (4.11)).

$$\hat{\sigma}^2 = \mu_{\sigma^2_{B_s}} = \frac{\sum_m \sigma^2_{B_s}}{m} \tag{4.11}$$

where, $\sigma^2_{B_s}$ is the variance of the selected homogeneous blocks, and *m* is the number of the selected blocks.

## 4.3 Experimental Results

As well known, the most challenging part for the structure-based noise estimation is how to distinguish where is the noise information and where is the image structure information. When the original image is relatively simple without much edge information, most algorithms perform similarly, estimating the noise variance well for range of noise levels [82]. However, when using a more complex image, with a lot of textured areas, the results change. For the most common case, part of edge information is also organized as the noise information. And the noise variance tends to be overestimated. Thus, in this Chapter, we only select the fine texture images (see Figure

(a)

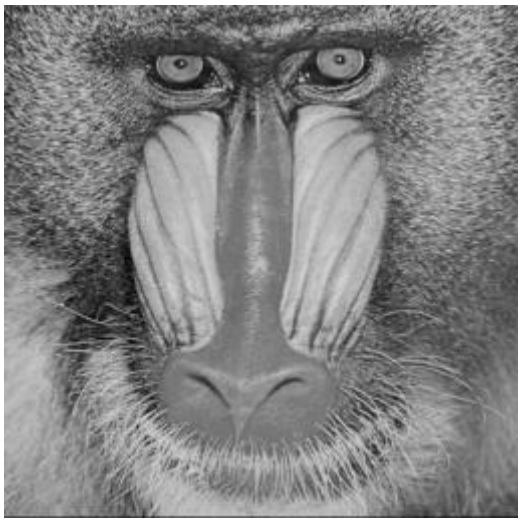

(b)

(c)

Figure 4.1 Fine texture images used for experiments
(a) Bridge, (b) Baboon, (c) Arial

4.1) for results comparison in order to show the significant improvement of the proposed method on rejecting the edge information. The original method in [52] is used for the comparison since it is also a structure-based method similar with the proposed method using different filter for block selection process.

To evaluate the performance of the proposed algorithm, the averages of noise standard deviation are first calculated to indicate the accuracy of the estimation (see (4.12)), and then, the averages of estimation errors are computed to check the stability (see (4.13)) of every noise level:

$$\mu_{\hat{\sigma}} = \frac{\sum_{n} \hat{\sigma}}{n} \tag{4.12}$$

where $\hat{\sigma}$ is the noise standard estimation result of a certain image and one estimation, $n$ is the number of estimations.

$$\mu_{E_\sigma} = \frac{\sum_{n} |\hat{\sigma} - \hat{\sigma}_T|}{n} \tag{4.13}$$

where $\hat{\sigma}_T$ is the true noise standard deviation value and $\mu_{E_\sigma}$ is the average estimation error.

### 4.3.1 Results of Homogeneous Pixels Selection

First, Experiment results of homogeneous pixels selection are shown in Figures 4.2, 4.3 and 4.4. We take the noise level $\sigma = 20$ as an example (see Figures 4.2(a), 4.3(a) and 4.4(a)). We select the homogeneous area from the noisy images using the threshold based difference eigenvalue edge detector. And the corresponding results are shown in Figures 4.2(b), 4.3(b) and 4.4(b), respectively. As can be seen, the performance is effective and only the homogeneous pixels are selected (white color pixels) with the edge information well rejected. And this leads to the more accuracy estimation results reported in Section 4.3.2.

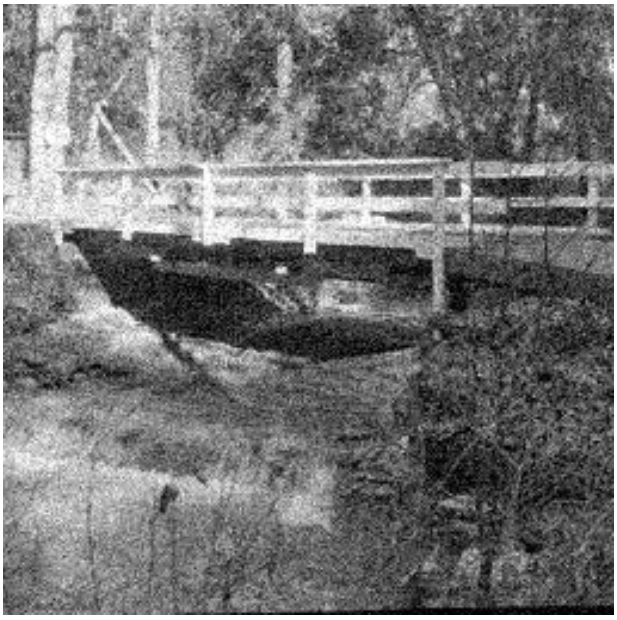

(a)

(b)

Figure 4.2 Noisy image - Bridge ( $\sigma = 20$ ) and the selected pixels for noise estimation: (a) Noisy image: Bridge (b) Selected homogeneous pixels (white pixels)

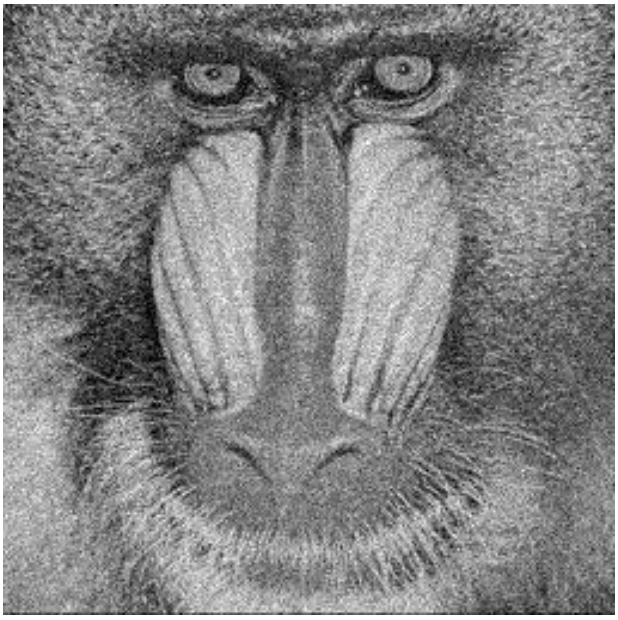

(a)

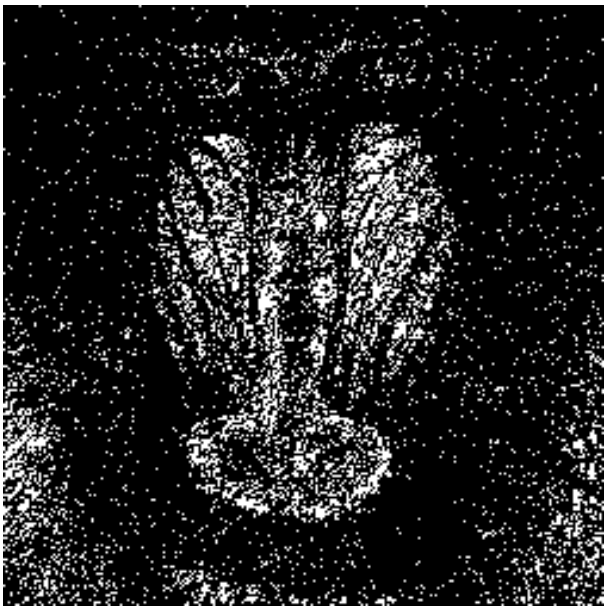

(b)

Figure 4.3 Noisy image - Baboon ( $\sigma = 20$ ) and the selected pixels for noise estimation: (a) Noisy image: Baboon (b) Selected homogeneous pixels (white pixels)

(a)

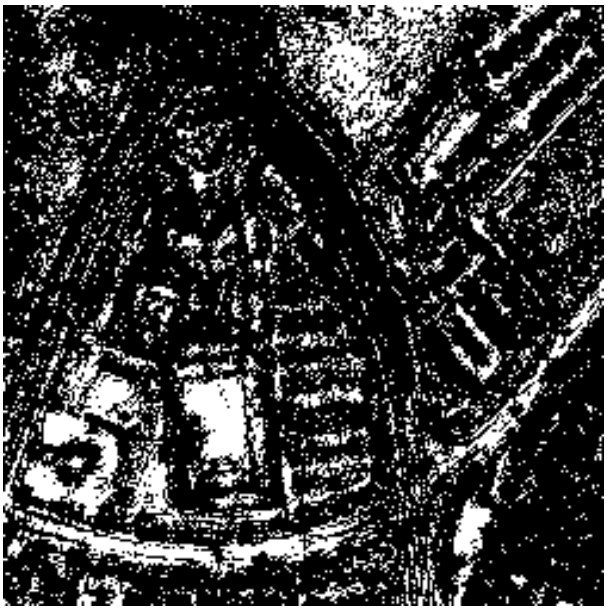

(b)

Figure 4.4 Noisy image - Arial ( $\sigma = 20$ ) and the selected pixels for noise estimation: (a) Noisy image: Arial (b) Selected homogeneous pixels (white pixels)

### 4.3.2 Comparison Results

Comparison results using three images are shown in Figures 4.5, 4.6 and 4.7, respectively.

In Figures 4.5(a), 4.6(a) and 4.7(a), the black line ‘true’ corresponds to the true data of the noise standard deviation, that is, estimation without error. This is used to describe the distance between the estimated results and true data. As shown in Figures 4.5(a), 4.6(a) and 4.7(a), the estimated results for the proposed masks outperform the original ones for most noise levels and the estimation results of ‘Arial’ from 15 to 30 is quite similar to the true data (see Figure 4.7(a)).

The estimation error for the proposed method is lower significantly for most noise levels other than the similar result at 20 dB (see Figures 4.5(b), 4.6(b) and 4.7(b)).

## 4.4 Summary

We proposed a reliable method for noise variance estimation in noisy images. This method utilized the difference eigenvalue edge indicator adding a proper threshold to select the homogeneous areas in the noisy image. Only the blocks including only homogeneous pixels were used for the next averaging step. The proposed method outstood the original method significantly and reveals better stability for estimation at most noise levels. Experiments with fine texture images were described. Experimental results demonstrated that our method is feasible and effective for noise variance estimation, especially for fine texture images.

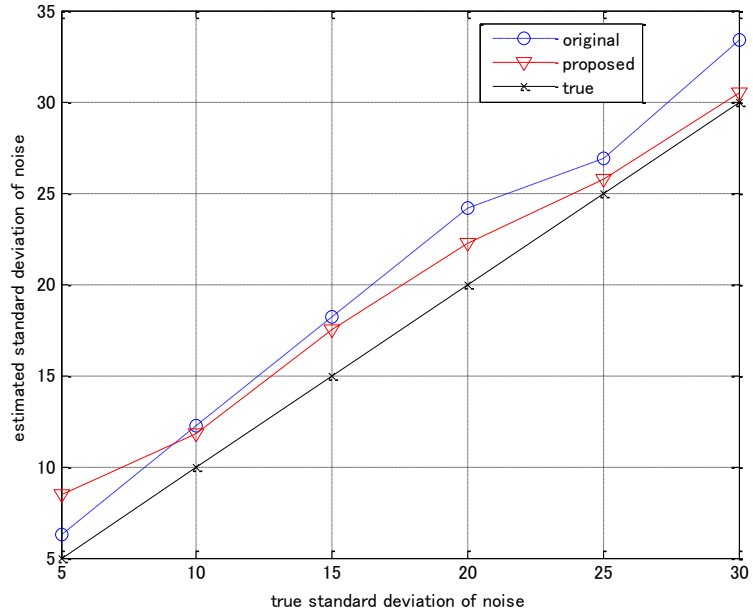


(a)

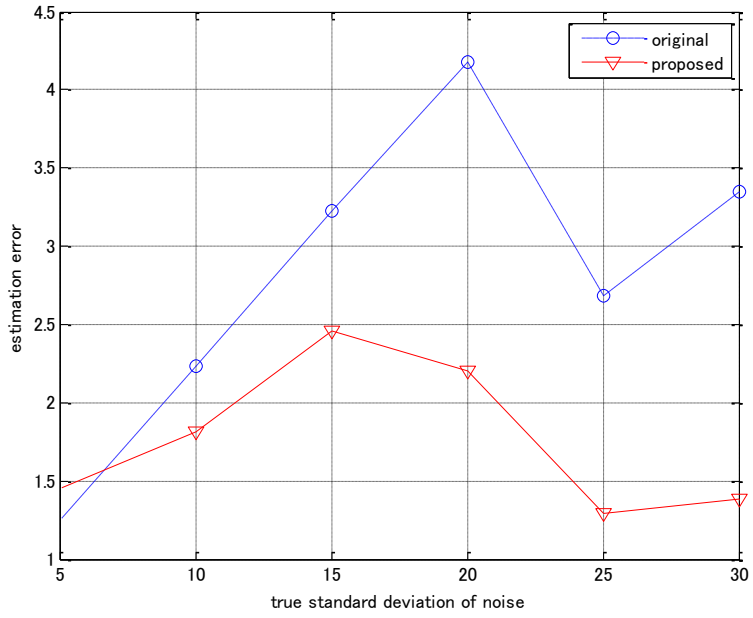


(b)

Figure 4.5　Comparison of original method and proposed method using ‘Bridge’
(a) Average of estimation results, (b) Average of estimation error

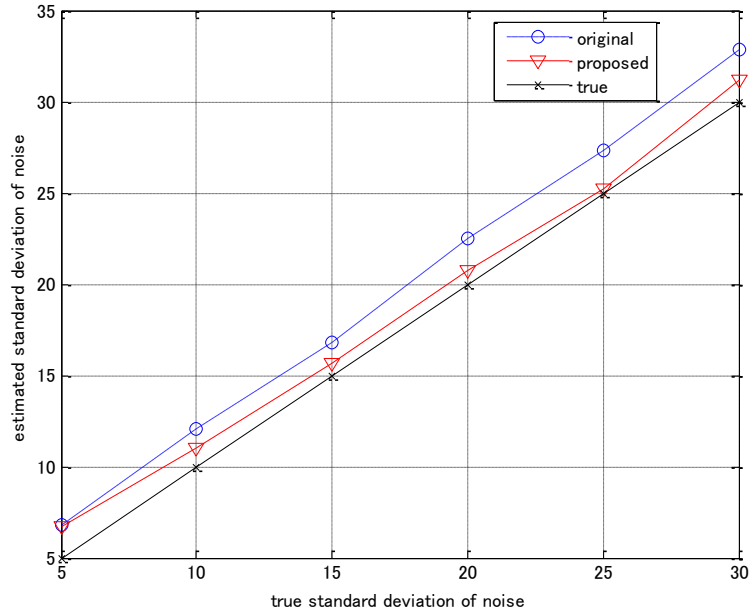


(a)

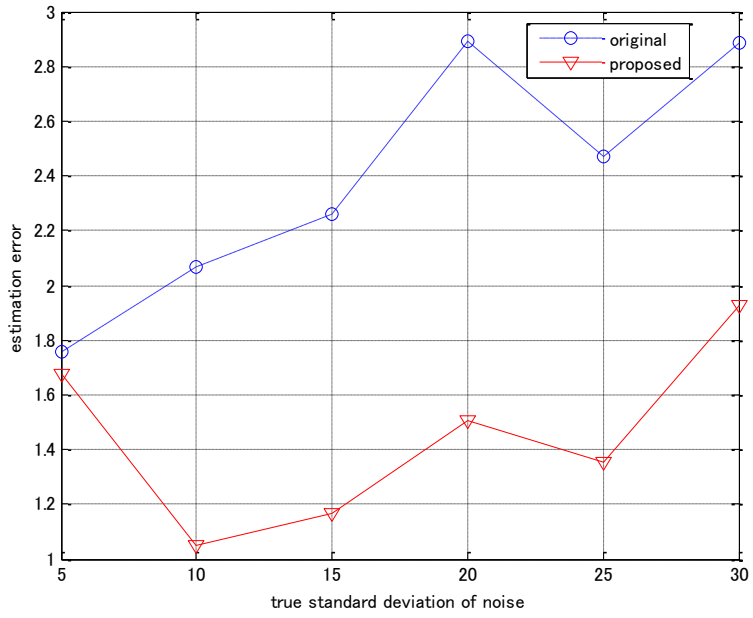


(b)

Figure 4.6 Comparison of original method and proposed method using 'Baboon': (a) Average of estimation results, (b) Average of estimation error

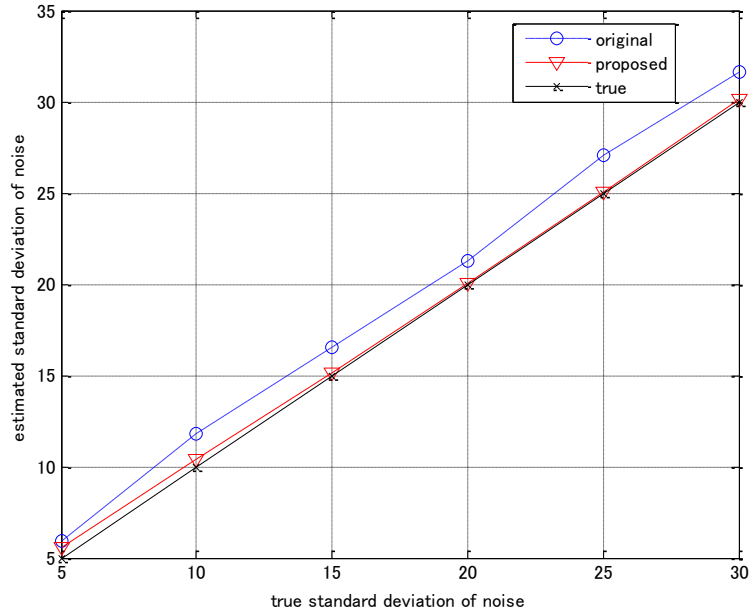


(a)

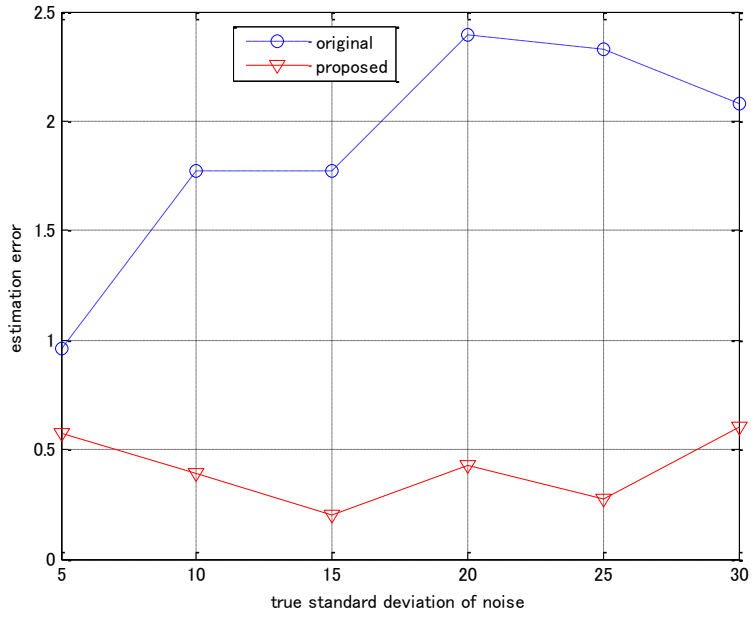


(b)

Figure 4.7　Comparison of original method and proposed method using ‘Arial’: (a) Average of estimation results, (b) Average of estimation error

Chapter 5

# 5 Conclusions

This Chapter concludes the thesis with a summary of our work. The future research is also stated in this Chapter.

## 5.1 Summary of the Research

The technique of blind image restoration estimating both the true image and the blur from degraded image has been researched in recent years. However, when taking noise into account, the estimation problem becomes more challenging. Estimating the blue and noise parameters simultaneously may cause a large estimation error.

Thus, in order to minimize the estimation error, we proposed a Maximum-Likelihood Estimation Algorithm based on noise variance estimation. Different from the original method, this method separates the estimation parameters into three parts, and estimates the noise variance not using the estimated blur coefficients but using the known degraded image. This improves the estimation accuracy significantly and leads to the higher PSNR of the final restoration results.

Since the noise estimation process is a very important task for the previous restoration method of this thesis, we further proposed a structure-based method from the degraded image for better results of noise variance estimation. This method separates an image into blocks. Rejecting the edge included block, only homogenous blocks are selected for the noise estimation process.

Comparing several filters for the homogenous blocks selection in one image, we finally find that image details can be better revealed by second-order operators. Thus,

for better results of noise estimation, we further proposed a difference eigenvalue based edge indicator with threshold for more accurate block selection, which leads to the better noise estimation results.

After embedding the proposed noise variance estimation into the image restoration, we can see some improvements. Firstly, the original ML method can only provide the accurate estimation results of blur and noise parameters for the case of middle size of blur. As described in the Chapter 2, noise variance is calculated using the estimated blur parameters. Thus, the error of noise estimation tends to be amplified by the error of blur estimation. But the embedded noise estimation methods estimating the noise variance only using the degraded image in Chapters 3 and 4 change this situation. As a result, the noise estimation is robust for both heavy and light blur conditions. Better estimations lead to the better restoration results obviously. Secondly, we have better choice for restoration of different kinds of images. For example, for the homogenous or lightly noisy images, we can select the proposed ML method embedding the noise estimation method in Chapter 3; else, for the fine texture or heavily noisy image, we can select the ML method embedding the noise estimation method in Chapter 4, respectively.

Furthermore, we notice that the noise estimation methods shown in Chapters 3 and 4 can also be used independently. Since noise estimation is also an important issue for image processing and can be used as an essential preprocessing in many image processing systems, it is expected that the noise estimation methods in Chapters 3 and 4 play an important role to improve the performance of image processing systems.

## 5.2 Future Works

The research in this thesis has led to some interesting developments in blind image deconvolution and noise estimation. However, some problems still exist. The image restoration method in Chapter 2 is an iteration method, which depends on proper initial values. The two noise estimation methods in Chapters 3 and 4 have different property. The method in Chapter 3 is more effective to the good quality images, while the method in Chapter 4 is more effective to the fine texture images. Therefore, we believe that a well engineered solution of these problems will most likely be formed in the future.

# Bibliography

[1] D. Kundur and D. Hatzinakos: Blind image deconvolution, IEEE Signal Processing Magazine, Vol. 13, No. 3, pp. 43-64, May 1996.

[2] A. K. Katsaggelos, ed.: Digital Image Restoration, New York: Springer-Verlag, 1991.

[3] H. C. Andrews and B. R. Hunt: Digital Image Restoration, New Jersey: Prentice-Hall, 1997.

[4] R. H. T. Bates: Astronomical speckle imaging, Physics Reports., Vol. 90, No. 4, pp.203-297, 1982.

[5] J. P. Muller, ed.: Digital image processing in remote sensing, Philadelphia: Taylor & Francis, pp. 226-269, 1988.

[6] K. Faulkner, C. J. Kotre and M. Louka: Veiling glare deconvolution of images produced by x-ray image intensifiers, Proc. IEEE International Conf. on Image Processing and Its Applications, pp. 669-673, 1989.

[7] T. Wilson and S. J. Hewlett: Imaging strategies in three-dimensional confocal microscopy, Proc. SPIE Conf. on Biomedical Image Processing, pp.35-45, 1990.

[8] S. N. Drossos: Fast artifact free reconstruction algorithm for limited data (PET) using constrained optimization, Proc. IEEE International Conf. on Image Processing and Its Application, pp. 367-372, 1989.

[9] V. Krishnamurthi, Y. Liu and T. J. Holmes: Blind deconvolution of 2D and 3D fluorescent micrographs, Proc. SPIE Conf. on Biomedical Image Processing and Three-Dimensional Microscopy, pp. 95-102, 1992.

[10] A. K. Jain and S. Ranganath: Applications of two dimensional spectral estimation in image restoration, Proc. IEEE Conf. on Acoustics, Speech and Signal Processing, pp. 1113-1116, 1981.

[11] B. R. Hunt: The application of constrained least squares estimation to image restoration by digital computer, IEEE Trans. on Computers, Vol. C-22, No. 9, pp. 805-812, 1973.

[12] A. O. Aboutalib and L. M. Silverman: Restoration of motion degraded images, IEEE Trans. on Circuits and Systems, Vol. 22, No. 3, pp. 278-286, 1975.

[13] J. Biemond, R. L. Lagendijk, and R. M. Mersereau: Iterative methods for image deblurring, Proc. IEEE, Vol. 78, No. 5, pp. 856-883, 1990.

[14] T. J. Schulz: Multiframe blind deconvolution of astronomical images, Journal of Optical Society America A, Vol. 10, No. 5, pp. 1064-1073, 1993.

[15] T. Dennis, R. D. Start, and S. S. Cross: The use of digital imaging, video conferencing, and telepathology in histopathology: a national survey, Journal of Clinical Pathology, Vol. 58, No. 3, pp. 254-258, 1993.

[16] A. G. Qureshi and H. T. Mouftah: Partially-blind image restoration using constrained Kalman filtering, Proc. IEEE Conf. on Acoustics, Speech, Signal Processing, pp. 3713-3716, 1991.

[17] P. Nisenson and R. Barakat: Partial atmospheric correction with adaptive optics, Journal of Optical Society America A, Vol. 4, No. 12, pp. 2249-2253, 1991.

[18] M. C. Roggemann: Limited degree-of-freedom adaptive optics and image reconstruction, Applied Optics, Vol. 30, No. 29, pp. 4227-4233, 1991.

[19] R. A. Wiggins: Minimum entropy deconvolution, Geoexploration, Vol. 16, No. 1-2, pp. 21-35, 1978.

[20] S. Haykin, ed.: Blind Deconvolution, New Jersey: Prentice-Hall, 1991.

[21] J. L. Yen: Array Signal Processing, New Jersey: Prentice-Hall, 1985.

[22] N. B. Karayiannis and A. N. Venetsanopoulos: Regularization theory in image restoration: the regularizing operator approach, Optical Engineering, Vol. 28, No. 7, pp. 761-780, 1989.

[23] R. G. Lane and R. H. T. Bates: Automatic multidimensional deconvolution, Journal of Optical Society America A, Vol. 4, No. 1, pp. 180-188, 1987.

[24] I. S. Stefanescu: On the phase retrieval problem in two dimensions, Journal of Mathematical Physics, Vol. 26, No. 9, pp. 2141-2160, 1985.

[25] M. Cannon: Blind deconvolution of spatially invariant image blurs with phase, IEEE Trans. on Acoustics, Speech, Signal Processing, Vol. 24, No. 1, pp. 58-63, 1976.

[26] M. M. Chang, A. M. Tekalp and A. T. Erdem: Blur identification using the bispectrum, IEEE Trans. on Signal Processing, Vol. 39, No. 10, pp. 2323-2325, 1991.

[27] B. Chalmond: PSF estimation for image deblurring, CVGIP: Graphical Models and Image Processing, Vol. 53, No. 4, pp. 364-372, 1991.

[28] R. Fabian and D. Malah: Robust identification of motion and out-of-focus blur parameters from blurred and noisy images, CVGIP: Graphical Models and Image Processing, Vol. 53, No. 5, pp. 403-412, 1991.

[29] A. M. Tekalp, H. Kaufman and J. W. Woods: Identification of image and blur parameters for the restoration of noncausal blurs, Proc. IEEE Conf. on Acoustics, Speech and Signal Processing, pp. 963-972, 1986.

[30] R. L. Lagendijk, A. M. Tekalpo and J. Biemond: Maximum likelihood image and blur identification: a unifying approach, Optical Engineering, Vol. 29, No. 5, pp. 422-435, 1990.

[31] R. L. Lagendijk, J. Biemond and D. E. Boekee: Hierarchical blur identification, Proc. IEEE Conf. on Acoustics, Speech, Signal Processing, pp. 1889-1892, 1990.

[32] R. L. Lagendijg, J. Biemond and D. E. Boekee: Identification and restoration of noisy blurred images using the expectation-maximization algorithm, IEEE Trans. on Acoustics, Speech and Signal Processing, Vol. 38, No. 7, pp. 1180-1191, 1990.

[33] S. J. Reeves and R. M. Mersereau: Blur identification by the method of generalized cross-validation, IEEE Trans. on Image Processing, Vol. 1, No. 3, pp. 301-311, 1992.

[34] C. M. Cho and H. S. Don: Blur identification and image restoration using a multilayer neural network, Proc. IEEE Conf. on Neural Networks, pp. 2558-2563, 1991.

[35] C. L. Nikias and A. P. Petropulu: Higher-Order Spectral Analysis, A Nonlinear Processing Framework, Prentice Hall, pp. 282-295, 1991.

[36] M. K. Ng, R. J. Plemmons: Regularization of RIF blind image deconvolution, IEEE Trans. on Image Processing, Vol. 9, No. 6, pp. 1130-1134, 2000.

[37] D. Kundur and D. Hatzinakos: A novel blind deconvolution scheme for image restoration using recursive filtering, IEEE Trans. on Signal Processing, Vol. 46, No. 2, pp. 375-390, 1998.

[38] H. S. Wu: Minimum entropy deconvolution for restoration of blurred two-tone images, Electronics Letters, Vol. 26, No. 15, pp. 1183-1184, 1990.

[39] G. Jacovitti and A. Neri: A Bayesian approach to 2D non minimum phase AR identification, Proc. ASSP Workshop on Spectrum Estimation and Modeling, pp. 79-83, 1990.

[40] J. L. Zhuang and Y. S. Xia: A two-dimensional iterative algorithm for blind image restoration based on an L1 regularization approach, Proc. IEEE International Congress on Image and Signal Processing, pp. 51-55, 2010.

[41] X. J. Bi and T. Wang: Adaptive blind image restoration algorithm of degraded image, Proc. IEEE Congress on Image and Signal Processing, pp. 536-540, 2008.

[42] X. Z. Liu, M. J. Li, H. J. Zhang and D. X. Wang: Bayesian motion blur identification using blur priori, Proc. IEEE Conf. on Image Processing, pp. 957-960, 2003.

[43] H. W. Sun, M. Desvignes, Y. H. Yan and W. W. Liu: Motion blur parameters identification from radon transform image gradients, Proc. IEEE Conf. on Industrial Electronics, pp. 2098-2103, 2009.

[44] L. Cui, W. R. Ding, Y. Y. Man and D. Wang: Restoration of defocus blur image based on global phase coherence, Proc. IEEE International Congress on Image and Signal Processing, pp. 1-5, 2009.

[45] J. S. Lee, A. S. Fathi and S. Song: Defocus blur estimation using a cellular neural network, Proc. IEEE International Workshop on Cellular Nanoscale Networks and Their Applications, pp. 1-4, 2010.

[46] F. Chen and J. L. Ma: An empirical identification method of Gaussian blur parameter for image deblurring, IEEE Trans. on Signal Processing, Vol. 57, No. 7, pp. 2467-2478, July 2009.

[47] F. Orieux, J. F. Giovannelli and T. Rodet: Deconvolution with Gaussian blur parameter and hyperparameters estimation, Proc. IEEE International Conf. on Acoustics Speech and Signal Processing, pp. 1350-1353, 2010.

[48] P. Campisi and K. Egiazarian: Blind Image Deconvolution: Theory and Applications, CRC Press, 2007.

[49] L. Chen and K. H Yap: A soft double regularization approach to parametric blind image deconvolution, IEEE Trans. on Image Processing, Vol. 14, No. 5, pp. 624-633, May 2005.

[50] P. D. Wirawan, and H. Maitre: Multi-channel high resolution blind image restoration, IEEE International Conf. on Acoustics, Speech, and Signal Processing, pp. 3229-3232, 1999.

[51] Z. P. Deng and Y. S. Xia: A neural network algorithm for fast blind image restoration using a novel 2D-ARMA parameter estimation, Proc. IEEE International Conf. on Audio Language and Image Processing, pp. 1744-1748, 2010.

[52] A. Amer and E. Dubois: Fast and reliable structure-oriented video noise estimation, IEEE Trans. on Circuits and Systems for Video Technology, Vol. 15, No. 1, pp. 113-118, January 2005.

[53] Z. J. Pei, Q. Q. Tong, L. N. Wang and J. Zhang: A median filter method for image noise variance estimation, Proc. IEEE Conf. on Information Technology and Computer Science, pp. 13-16, 2010.

[54] S. Beheshti and M. A. Dahleh: Noise variance in signal denoising, Proc. IEEE International Conf. on Acoustics, Speech, and Signal Processing, pp. 185-188, 2003.

[55] W. K. Pratt: Vector space formulation of two-dimensional signal processing operations, Computer Graphics and Image Processing, Vol. 4, No. 1, pp. 1-24, 1975.

[56] S. J. Reeves and R. M. Mersereau: Blur identification by the method of generalized cross-validation, IEEE Trans. on Image Processing, Vol. 1, No. 3, pp. 301-311, July 1992.

[57] S. Q. Wu, Z. K. Lu, E. P. Ong and W. S. Lin: Blind image blur identification in cepstrum domain, Proc. IEEE International Conf. on Computer Communications and Networks, pp. 1166-1171, 2007.

[58] X. Q. Su, X. Li and L. Ji: Blind image restoration based on automatic blur identify and total variation minimization, Proc. IEEE International Conf. on Mechanic Automation and Control Engineering, pp. 2943-2946, 2010.

[59] L. Chen and K. H. Yap: Identification of blur support size in blind image deconvolution, Proc. IEEE International Conf. on Information, Communication and Signal Processing, pp. 503-507, 2003.

[60] D. Lowe: Object recognition from local scale-Invariant features, Proc. IEEE Conf. on Computer Vision, pp. 1150-1157, 1999.

[61] D. Robinson and P. Milanfar: Fundamental performance limits in image registration, IEEE Trans. on Image Process, Vol. 13, No. 9, pp. 1185-1199, 2004.

[62] P. P. Rayan Kutty and A. Sreenivasa Murthy: Kalman filter using quantile based noise estimation for audio restoration, Proc. IEEE Conf. on Emerging Trends in Electrical and Computer Technology, pp. 616-620, 2011.

[63] C. H. Li, K. He and J. L. Zhou: Edge detection of image on the local feature, Proc. IEEE Symposium on Intelligent Information Technology Application, pp. 326-330, 2008.

[64] X. B. Wang: Image edge detection based on lifting wavelet, Proc. IEEE Conf. on Intelligent Human-Machine Systems and Cybernetics, pp. 25-27, 2009.

[65] L. X. Jiang, W. J. Zhou and Y. Wang: Study on improved algorithm for image edge detection, Proc. IEEE Conf. on Computer and Automation Engineering, pp. 476-479, 2010.

[66] M. E. Farmer and A. K. Jain: A wrapper-based approach to image segmentation and classification, IEEE Trans. on Image Processing, Vol. 14, No. 12, pp. 2060-2072, 2005.

[67] J. Tang: A color image segmentation algorithm based on region growing, Proc. IEEE Conf. on Computer Engineering and Technology, pp. 634-637, 2010.

[68] H. Zhang, Q. Y. Zhu and X. F. Guan: Probe into image segmentation based on Sobel operator and maximum entropy algorithm, Proc. IEEE Conf. on Computer Science and Service System, pp. 238-241, 2012.

[69] K. P. Wong: Fractal image coding for emission tomographic image compression, Proc. IEEE Symposium on Nuclear Science, pp. 1376-1379, 2001.

[70] P. Y. Wu: Distributed fractal image compression on PVM for million-pixel images, Proc. IEEE Conf. on Information Networking, pp. 393-398, 2001.

[71] P. Suapang, K. Dejhan and S. Yimmun: A web-based DICOM-format image archive, medical image compression and DICOM viewer system for teleradiology Application. Proc. IEEE SICE Annual Conf., pp. 3005-3011, 2010.

[72] K. Rank, M. Lendl and R. Unbehauen: Estimation of image noise variance, Proc. IEEE Conf. on Vision, Image and Signal Processing, pp. 80-84, 1999.

[73] R. C. Bilcu and M. Vehvilainen: A new method for noise estimation in images, Proc. IEEE EURASIP International Workshop on Nonlinear Signal and Image Processing, pp. 18-20, 2005.

[74] W. J. Liu, T. Liu, M. T. Rong, R, L. Wang and H. Zhang: A fast noise variance estimation algorithm, Proc. IEEE Conf. on Postgraduate Research in Microelectronics and Electronics, pp. 61-64, 2011.

[75] D. H. Shin, R. H. Park, S. J. Yang and J. H. Jung: Block-based noise estimation using adaptive Gaussian filtering, IEEE Trans. on Consumer Electronics, Vol. 51, No. 1, pp. 218-226, 2005.

[76] X. Liu, M. Tanaka and M. Okutomi: Noise level estimation using weak textured patches of a single noisy image, Proc. IEEE Conf. on Image Processing, pp. 665-668, 2012.

[77] G. Zhai and X. Wu: Noise estimation using statistics of natural images, Proc. IEEE Conf. on Image Processing, pp. 1857-1860, 2011.

[78] D. Zoran and Y. Weiss: Scale invariance and noise in natural images, Proc. IEEE Conf. on Computer Vision, pp. 2209-2216, 2009.

[79] R. A. and S. Z. Carmona: Adaptive smoothing respecting feature directions, IEEE Trans. on Image Processing, Vol. 7, No. 3, pp. 353-358, 1998.

[80] M. Lysaker: Iterative image restoration combining total variation minimization and a second-order functional, Journal of Computer Vision, Vol. 66, No. 1, pp. 5-18, 2006.

[81] C. Tand, L. Han, H. Ren, D. Zhou, Y, Chang, X. Wang and X. Cui: Second-order oriented partial-differential equations for denoising in electronic-speckle-pattern interferometry fringes, Optics Letters, Vol. 33, No. 19, pp. 2179-2181, 2008.

[82] H. Tian, H. Cai, J. H. Lai and X. Xu: Effective image noise removal based on difference eigenvalue, Proc. IEEE Conf. on Image Processing, pp. 3357-3360, 2011.

# Publications

## Journal Papers

[J1] C. Yi and T. Shimamura, "An Improved Maximum-Likelihood Estimation Algorithm for Blind Image Deconvolution Based on Noise Variance Estimation," Journal of Signal Processing, Vol. 16, No. 6, pp. 629-635, 2012.

[J2] C. Yi and T. Shimamura, "An Improved Structure-Based Gaussian Noise Variance Estimation Method for Noisy Images," Journal of Signal Processing, Vol. 17, No. 6, pp. 299-305, 2013.

## Conference Papers

[C1] C. Yi and T. Shimamura, "A Blind Image Deconvolution Method Based on Noise Variance Estimation and Blur Type Reorganization," Proc. IEEE International Conf. on Intelligent Signal Processing and Communications Systems, 6 pages, 2011.

[C2] C. Yi and T. Shimamura, "Improved Structure-Based Noise Variance Estimation for Noisy Images," Proc. IEEE International Symposium on Signal Processing and Information Technology, 5 pages, 2012.

[C3] C. Yi and T. Shimamura, "Improved Structure-Based Noise Variance Estimation," Proc. WSEAS International Conf. on Applied Computer Science, pp. 27-33, 2012.